Cell Reports

Article

Immunodominant surface epitopes power immune evasion in the African trypanosome

Graphical abstract

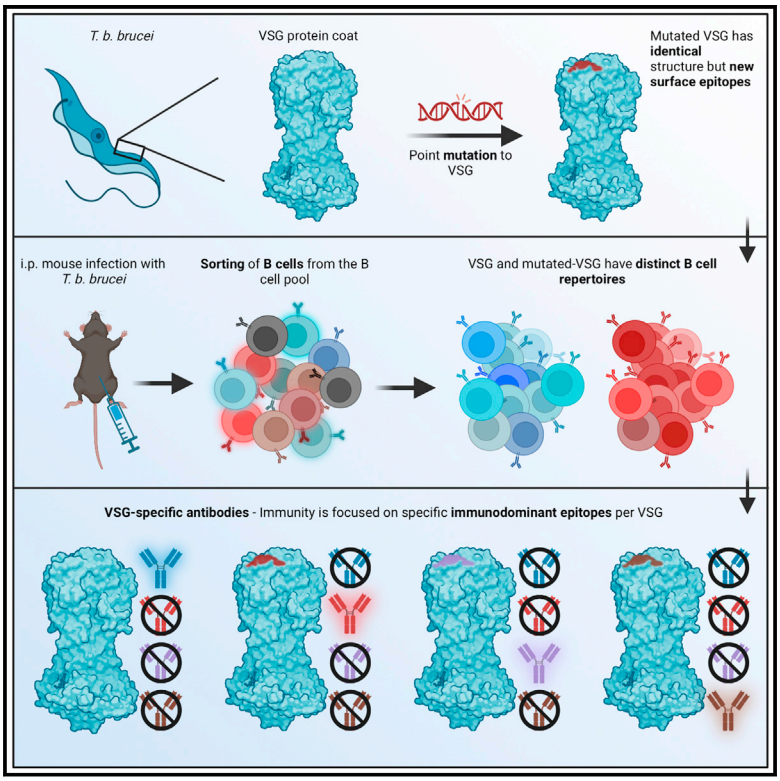

Highlights

- Mutated VSGs are identical in structure but elicit distinct antibody repertoires
- Antibody repertoires elicited by the same VSGs are highly stereotyped between mice
- Host immunity is focused on a restricted set of immunodominant epitopes per VSG

Authors

Anastasia Gkeka, Francisco Aresta-Branco, Gianna Triller, ..., Joseph P. Verdi, C. Erec Stebbins, F. Nina Papavasiliou

Correspondence

e.stebbins@dkfz-heidelberg.de (C.E.S.), n.papavasiliou@dkfz-heidelberg.de (F.N.P.)

In brief

Gkeka et al. analyze the antibody response to different surface proteins of the African trypanosome. They determine that it is restricted and targeted to specific surface epitopes. They also show that minor changes in these epitopes trigger a different response, allowing *T. brucei* to focus host immunity on those epitopes and prolonging immune evasion.

Gkeka et al., 2023, Cell Reports *42*, 112262
March 28, 2023
https://doi.org/10.1016/j.celrep.2023.112262

CellPress

Cell Reports

CellPress
OPEN ACCESS

Article

Immunodominant surface epitopes power immune evasion in the African trypanosome

Anastasia Gkeka,[1,2,4,9] Francisco Aresta-Branco,[1,3,9] Gianna Triller,[1] Evi P. Vlachou,[1] Monique van Straaten,[3] Mirjana Lilic,[5] Paul Dominic B. Olinares,[6] Kathryn Perez,[7] Brian T. Chait,[6] Renata Blatnik,[8] Thomas Ruppert,[8] Joseph P. Verdi,[1,4] C. Erec Stebbins,[3,*] and F. Nina Papavasiliou[1,10,*]
[1]Division of Immune Diversity, German Cancer Research Center, 69120 Heidelberg, Germany
[2]Faculty of Biosciences, University of Heidelberg, 69120 Heidelberg, Germany
[3]Division of Structural Biology of Infection and Immunity, German Cancer Research Center, 69120 Heidelberg, Germany
[4]Panosome GmbH, 69123 Heidelberg, Germany
[5]Laboratory of Structural Microbiology, the Rockefeller University, New York, NY 10065, USA
[6]Laboratory of Mass Spectrometry and Gaseous Ion Chemistry, the Rockefeller University, New York, NY 10065, USA
[7]Protein Expression and Purification Core Facility, EMBL Heidelberg, 69117 Heidelberg, Germany
[8]Center for Molecular Biology of Heidelberg University, DKFZ-ZMBH Alliance, 69120 Heidelberg, Germany
[9]These authors contributed equally
[10]Lead contact
*Correspondence: e.stebbins@dkfz-heidelberg.de (C.E.S.), n.papavasiliou@dkfz-heidelberg.de (F.N.P.)
https://doi.org/10.1016/j.celrep.2023.112262

SUMMARY

The African trypanosome survives the immune response of its mammalian host by antigenic variation of its major surface antigen (the variant surface glycoprotein or VSG). Here we describe the antibody repertoires elicited by different VSGs. We show that the repertoires are highly restricted and are directed predominantly to distinct epitopes on the surface of the VSGs. They are also highly discriminatory; minor alterations within these exposed epitopes confer antigenically distinct properties to these VSGs and elicit different repertoires. We propose that the patterned and repetitive nature of the VSG coat focuses host immunity to a restricted set of immunodominant epitopes per VSG, eliciting a highly stereotyped response, minimizing cross-reactivity between different VSGs and facilitating prolonged immune evasion through epitope variation.

INTRODUCTION

The African trypanosome (*Trypanosoma brucei* spp.) is a strictly extracellular parasite, infection with which elicits a robust antibody response against its variant surface glycoprotein (VSG) coat.[1,2] This response mediates parasite clearance, but is vulnerable to immune escape from variants that have switched surface coat composition.[3] The VSG protein consists of a large N-terminal domain (NTD) (approximately 350 amino acids) and a shorter C-terminal domain (approximately 100 amino acids), the latter being linked to the membrane via a GPI anchor.[4] It is speculated that the majority of immune epitopes are located on the top lobe of the NTD, which is highly accessible to the immune system; however, there are no antibody-VSG co-crystal structures available to support this hypothesis,[5–7] and recent studies have challenged this model.[8]

The dynamic interplay between VSG coat switching by trypanosomes and the B cell response of the host that they evade is central to the maintenance of chronic infection,[9] as the switched parasites proliferate and get eventually eliminated, but new populations expressing different VSGs appear, leading to distinctive waves of parasitemia that emerge at intervals of 5–8 days.[3,10] Consequently, each infection cycle lasts around 8 days, making the repertoire from that time point particularly important to the host-pathogen interaction.

Nonetheless, very little is known about the nature of the antibody response against the VSG coat. A small number of papers dating back to the 1990s revealed that acute infection with *T. brucei* leads to extraordinarily high levels of immunoglobulin M (IgM) in humans and in mice.[1] The antibody response has often been characterized as polyclonal and many of those antibodies are autoreactive.[1,11,12] However, these data are conceptualized in the context of a prolonged infection that itself is polyclonal in the VSG archetype. An understanding of the response to individual VSG variants in a controlled setting is therefore lacking, since the culmination of multiple separate responses to different VSGs would produce a "polyclonal" B cell output in the greater infection context. Importantly, immunization or exposure to specific VSG surface coats prevents later infection by cells expressing that same coat, indicating that coat-specific antibodies are produced during infection.[3,13]

To explore the parameters of the antibody response to *T. brucei*, we examined the antibody repertoires elicited by two specific VSGs. These were chosen to broadly represent the two primary VSG "classes": VSG2 (a class A VSG) and VSG3 (a class B VSG).[14] Herein, we demonstrate that the repertoires show restricted V-gene usage, which is highly reproducible

between animals and experiments. Moreover, we show that small alterations (e.g., point mutations) within VSG surfaces result in distinct repertoires, suggesting that antibodies elicited by VSGs are selective toward specific epitopes on the surface of each VSG, and can discriminate even between single amino acid changes. We speculate that this intense immune focusing of antibody responses to a very small number of epitopes per VSG may have evolved to reduce cross-reactivity between VSGs and to facilitate prolonged immune evasion.

RESULTS

Trypanosome infections lead to rapid plasma cell expansion

To generate the antibody repertoires, we infected animals with each specific VSG-expressing parasite, and either "cleared" the parasites with the anti-protozoan compound diminazene 4 days after infection, as infection is often rapidly lethal,[15] or allowed the animals to clear the trypanosomes naturally (whenever feasible) after the first peak of parasitemia (at which point the parasites that have switched VSG coats remain and seed the next peak of parasitemia). Initial analyses of infected C57BL/6 mice showed a robust expansion of plasma cells (Figures 1A and S1A). This expansion was common to all infections regardless of whether parasites were cleared by the animals (usually by day 6 or day 7 post infection) or whether they were pharmacologically cleared earlier with diminazene (days 4 and 5), allowing for the maturation of the antibody response until collection (at day 8 post infection; Figure 1B). This is also consistent with known parameters of disease progression.[3,16,17]

Typically, the characterization of an antigen-specific antibody repertoire benefits from the "baiting" of antigen-specific B cells using the antigen itself conjugated to a fluorophore (PE or APC).[18,19] However, plasma cells are notoriously hard to bait as they downregulate surface expression of Ig and rather secrete the vast majority of the antibody they produce, so that very little antibody remains surface bound and accessible. We therefore proceeded to sort all plasma cells according to surface marker expression (CD138+/CD19^{lo})[20] into 384-well plates. The antibody repertoire of plasma cells was then assembled after two rounds of single-cell PCR and paired heavy (IgH) and light (Igκ/λ) gene sequence analysis.[18]

The VSG2$_{WT}$ repertoire is characterized by a small number of heavy and light chain variable region genes

We first focused on the repertoire elicited by VSG2-coated parasites. Surprisingly for a non-baited repertoire, plasma cells elicited from mice infected with VSG2 were dominated by cells carrying only four VH + VL chain pairings (VH10.1.86 or VH10.3.91 with VL19-20 or VL19-14; Figure 1C). These combinations, which are absent in naive mice (Figure S1B), formed the plurality of the repertoire when mice were pharmacologically treated to remove trypanosomes 4 days after infection, but they became increasingly prevalent in repertoires of animals that cleared trypanosomes naturally a day before collection, and even more dominant in repertoires of animals that cleared the infection the day we collected plasma cells (Figure 1C). This suggests a rapid and robust response to the parasite, stereotyped and highly reproducible between mice (Figure S2), that may become increasingly diversified as more antigens become available after parasite lysis.

We reasoned that the repertoire we collected closest to natural clearance would contain the B cells likely expressing the most potent anti-coat-specific antibodies and proceeded to analyze it further. While dominated by cells expressing two distinct Ig heavy and Ig light chain gene pairs, the B cells elicited by VSG2-coated *T. brucei* were not monoclonal: each VH10 heavy and 19-20 or 19-14 light chain V region was joined to a set of DJ or J gene segments representing a wide swath of CDR3 variants (Figure 1D; Data S1 and S2). This lack of clonal expansion is also evident from the Shannon entropy index, which is a statistical sequence-based measure of clonality (Figure 1C, bottom of each Circos plot).

We therefore picked a small number of heavy and light chain pairs from the overrepresented V gene segments identified and proceeded to express them recombinantly as soluble antibodies in HEK293T cells. Indeed, 7 out of 11 of these antibodies are capable of binding live, VSG2-coated *T. brucei* (Figure 1D). We conclude that the VSG2-elicited plasma cell repertoire represents an oligoclonal expansion primarily of four variable region defined pairs, which are mostly unmutated (Figure 1D). The V gene signature that defines this repertoire is stereotyped between mice (Figures 1C and S2), suggesting both that the VSG2-specific paratope is likely located within highly specific variable regions of the antibody protein and that these antibodies are likely generated against a common immunodominant epitope.

The structure of VSG2$_{WT}$ contains a calcium binding pocket, which defines the immunodominant epitope

Epitope identification is often achieved by structural analyses of repertoire-defined antibodies together with the antigen that elicited them.[21] We therefore sought to crystallize VSG2$_{WT}$ (specifically, the larger, surface-exposed NTD of the VSG) together with VSG2$_{WT}$-specific Fab fragments. However, VSG protein and Fab were not able to stay together in gel filtration chromatography (Figures S3A and S3B) and all crystals obtained were of VSG2 alone (Figure S4C; Table S1), likely because most antibodies elicited by *T. brucei* infection are of the IgM isotype (Figures S5A–S5C)[1] and are likely of low affinity (but high avidity). These antibodies are thus unlikely to bind with high affinity when produced recombinantly as an IgG (or Fab) fragment (as current methods for the recombinant production of pentameric IgM are poorly optimized). Serendipitously, the crystals did allow us to re-solve the structure of VSG2 to much higher resolution compared with previous work,[22,23] with unexpected findings. The protein structure of VSG2 from these new crystals is nearly identical to that from the 1990 crystal form, with a root-mean-square deviation of 0.87 Å over 1,420 atoms of a monomer in the dimer (Figures 2A and S4A). However, in later stages of model refinement, unusually large electron density around solvent molecules was modeled effectively with calcium (Figures 2B and 2C), an ion not present in older structures likely due to the use of chelating agents in the purification from animal blood.[24,25] Calcium is octahedrally coordinated in VSG2 through a network of oxygen bonds: four from three consecutive amino acid side chains at the end of a β strand (bidentate-D208,

CellPress
OPEN ACCESS

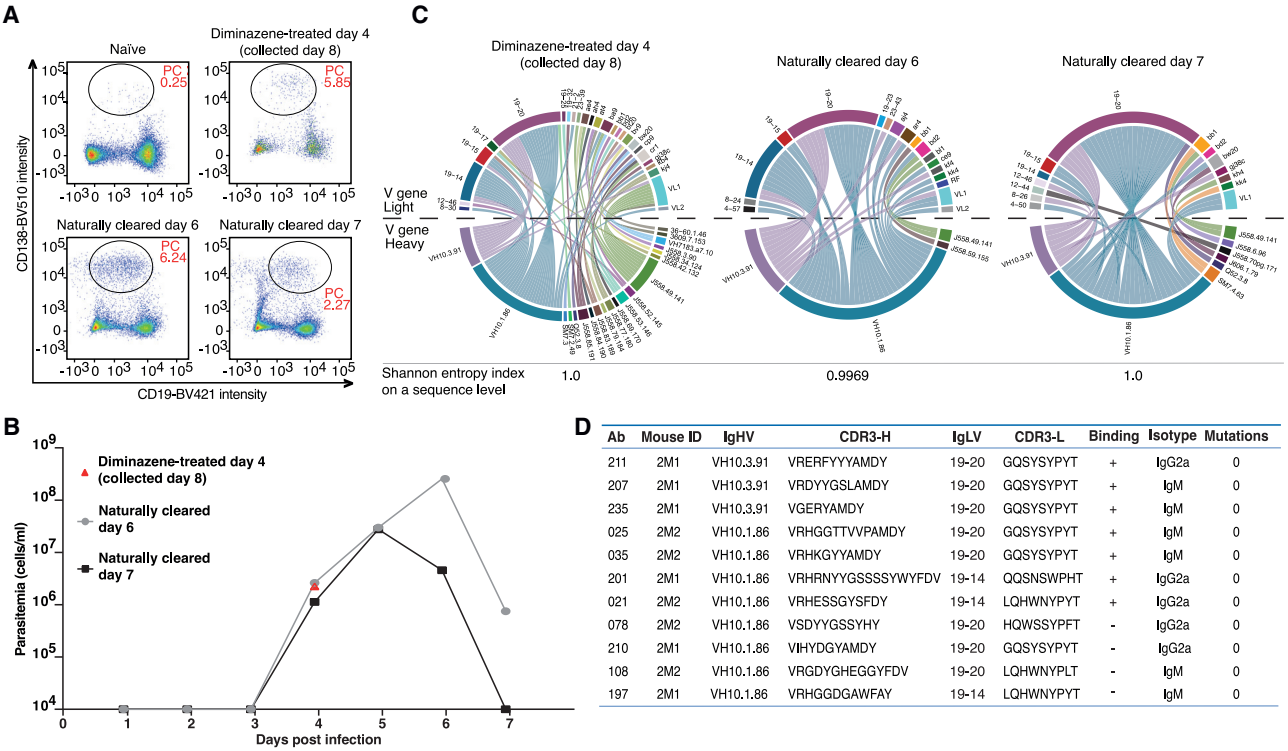

D

Ab	Mouse ID	IgHV	CDR3-H	IgLV	CDR3-L	Binding	Isotype	Mutations
211	2M1	VH10.3.91	VRERFYYYAMDY	19-20	GQSYSYPYT	+	IgG2a	0
207	2M1	VH10.3.91	VRDYYGSLAMDY	19-20	GQSYSYPYT	+	IgM	0
235	2M1	VH10.3.91	VGERYAMDY	19-20	GQSYSYPYT	+	IgM	0
025	2M2	VH10.1.86	VRHGGTTVVPAMDY	19-20	GQSYSYPYT	+	IgM	0
035	2M2	VH10.1.86	VRHKGYYAMDY	19-20	GQSYSYPYT	+	IgM	0
201	2M1	VH10.1.86	VRHRNYYGSSSSYWYFDV	19-14	QQSNSWPHT	+	IgG2a	0
021	2M2	VH10.1.86	VRHESSGYSFDY	19-14	LQHWNYPYT	+	IgG2a	0
078	2M2	VH10.1.86	VSDYYGSSYHY	19-20	HQWSSYPFT	-	IgG2a	0
210	2M1	VH10.1.86	VIHYDGYAMDY	19-20	GQSYSYPYT	-	IgG2a	0
108	2M2	VH10.1.86	VRGDYGHEGGYFDV	19-20	LQHWNYPLT	-	IgM	0
197	2M1	VH10.1.86	VRHGGDGAWFAY	19-14	LQHWNYPYT	-	IgM	0

Figure 1. $VSG2_{WT}$ parasites elicit a highly restricted antibody repertoire, defined by a small number of heavy and light chain pairs

(A) Percentage of CD138+ plasma cells (PC) within the live lymphocyte population in a non-infected naive mouse and in infected mice that were treated with diminazene or that naturally cleared the first peak of parasitemia. Plasma cells from this gate were sorted for antibody repertoire analysis. Three individual mice are shown for days 4, 6, and 7, as plots were identical for all mice in the experiment (n = 17). Representative gatings to determine live lymphocytes are shown in Figure S1A.

(B) Parasitemia infection curves from the two mice that naturally cleared the first peak of parasitemia (A) at day 6 (gray, n = 1) and day 7 (black, n = 1). Both mice were sacrificed at day 7 post-infection. A representative value of parasitemia at day 4 for mice treated with diminazene is indicated in red (n = 1).

(C) Circos plots generated for the $VSG2_{WT}$ V gene signatures of two independent mice (n = 2) whose infections were treated with diminazene (left, n = 96 pairs) and of two additional mice (n = 2) that naturally cleared the first peak of parasitemia at days 6 (center, n = 49 pairs) and 7 (right, n = 44 pairs) post infection. Different colors depict each heavy chain variable gene (bottom half of the plot), and each light chain variable gene (top half of the plot). The heavy and light chain variable gene pairings that form the antibodies are illustrated as connector lines starting from the heavy chain genes, providing also information about the frequency of the pairings. Genes from both chains that appeared only once and resulted in single heavy-light pairings, were considered background and were removed from the plot. Shannon entropy shows clonal diversity on a sequence level with a value of 1.0 representing 100% clonal diversity (no clones), while a value of 0.0 corresponding to 0% clonal diversity (only clones).

(D) Table with representative $VSG2_{WT}$ antibodies elicited in the context of diminazene-treated infections, which are mostly composed of VH10 heavy chains paired with 19–14 and 19-20 Vκ light chains. The CDR3 from each antibody is described, indicating that the repertoire is not monoclonal. The original antibody isotype, as well as somatic hypermutations, if any, are also shown.

N209, and D210, henceforth the "DND motif"), the carbonyl-oxygen from G155 in an opposing loop, and three water molecules in the solvent shell above the protein (each water coordinated by other side-chain and main-chain contacts from the protein, Figure 2C).

There is little change in the fold or amino acid side-chain positioning between the calcium bound and free structures of VSG2 (Figures 2A–2C), indicating that the pocket does not undergo any significant conformational changes upon calcium binding. The presence of calcium was verified both by mass spectrometry and isothermal titration calorimetry (Figures S6A–S6D). The calcium binding pocket in VSG2 appears to be unique, not closely resembling any published structures in the PDB (e.g., DALI homology search).[26] The pocket occurs near the "top" of the NTD of VSG2, slightly sheltered from the uppermost surface (Figure 2A). A triple mutation of the DND motif to alanine ($VSG2_{AAA}$) abrogates calcium binding (Figures S6E–S6G) without any significant conformational changes (Figures 2A, 2C, S4A, and S4D), although electrostatic surfaces generated from the three structures show an expected change to a more neutral charge distribution in the pocket region of the mutant (Figure 3A).

Unexpectedly, despite the high similarity between the wild-type and mutant structures, antisera elicited by infection with $VSG2_{WT}$-coated trypanosomes do not bind trypanosomes expressing the minor variant represented by the $VSG2_{AAA}$ mutant (Figure 3B). Furthermore, our recombinantly expressed antibodies specific to the $VSG2_{WT}$ coat were unable to bind the $VSG2_{AAA}$ mutant coat (Figure 3C), despite the fact that these mutations did not lead to any observable conformational differences in the crystallized protein. Interestingly, antibodies that

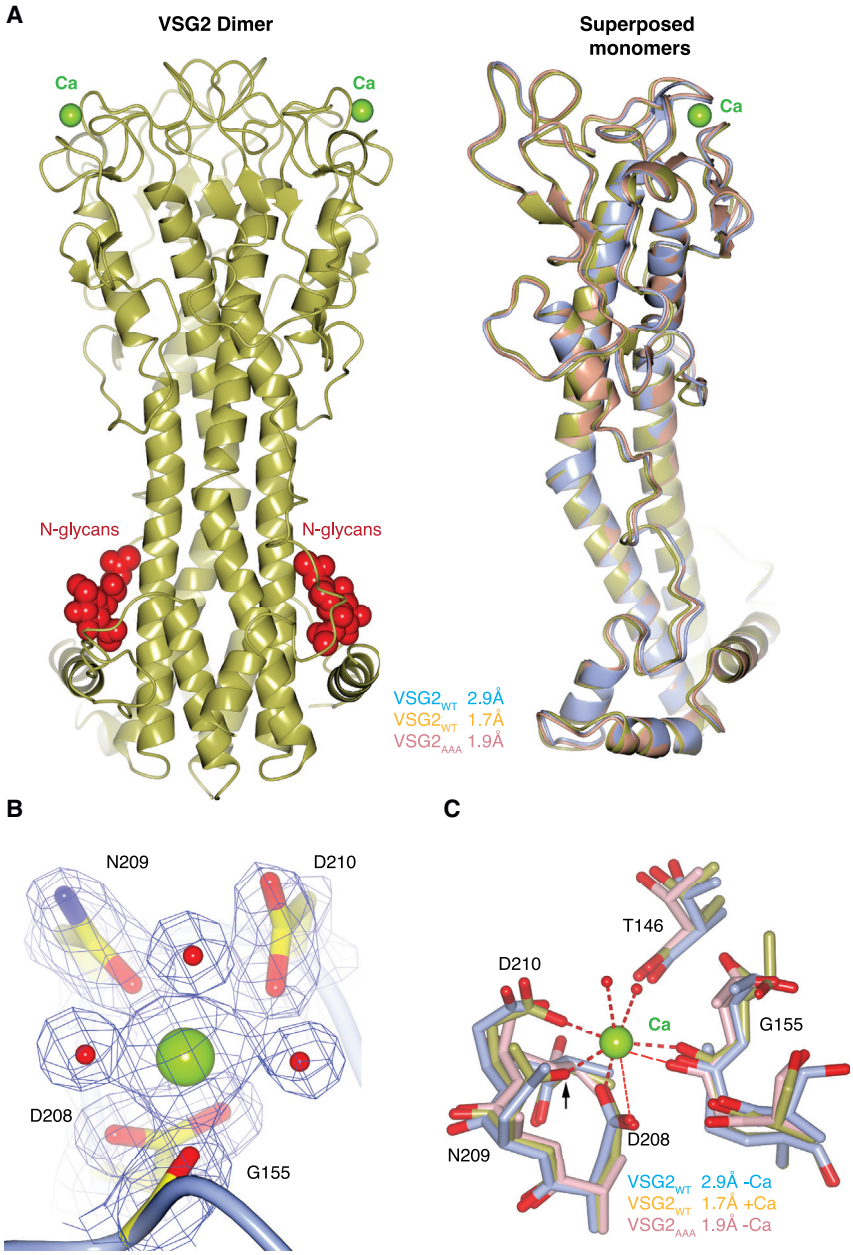

Figure 2. The resolved crystal structure of $VSG2_{WT}$ reveals the existence of a surface-exposed calcium binding pocket

(A) Left: crystal structure of $VSG2_{WT}$. The homodimer is shown as a ribbon diagram colored in gold, N-linked glycans and calcium atoms are displayed as red and green space-filling atoms, respectively. Right: structural alignment of monomers of $VSG2_{WT}$ (from left panel, in gold), $VSG2_{WT}$ (from Freymann et al.,[22] in blue) and $VSG2_{AAA}$ (in pink), highlighting the coordination of the calcium atom.

(B) Close-up of the coordination of calcium binding pocket with corresponding electron density maps. Water molecules and calcium atoms are displayed as red and green space-filling atoms, respectively.

(C) Superposition of the calcium binding pockets of the three structures presented in (A). Water molecules and calcium atoms are displayed as red and green space-filling atoms, respectively.

did not use the dominant V segments, including the next most represented combination (J558.49.141 + VL1) were not able to bind VSG2-coated parasites (both wild type and mutant) (Figures 3D and S7). These suggest that the VSG2 epitope recognized by both antisera and monoclonal antibodies is located within the region defined by the DND motif and, conversely, that antibodies to VSG2-coated trypanosomes are capable of a high degree of epitope discrimination.

The $VSG3_{S317A}$ repertoire is defined by a signature light chain V gene (gn33), absent from the wild type

To assess whether this combination of epitope immunodominance and antibody discrimination characterizes the epitope space of other VSGs, we analyzed antibody repertoires from plasma cells collected from animals infected with VSG3-coated trypanosomes. VSG3 is a member of a different VSG class with significant structural and post-translational modifications distinguishing it from VSG2 (class A vs. class B VSGs, respectively).[14] Previously, we had solved the crystal structure of the VSG3 NTD, leading to the unexpected identification of an *O*-linked glycosylation of a serine residue (S317, heterogeneously modified with 0-3 hexose residues) located in the center of the top surface of the protein.[27] Mutation of that serine to an alanine (S317A) residue ablated glycosylation, reduced parasite virulence, and enhanced the effectiveness of the host immune response.[27] At the time we hypothesized that this was due to the tendency of *O*-linked sugars to adopt multiple conformational states,[28] thus further diversifying the epitope space of the VSG3 coat. We sought to assess the validity of this hypothesis by analyzing plasma repertoires of $VSG3_{WT}$- and its S317 mutant ($VSG3_{S317A}$)-infected mice. Intriguingly, mice infected with $VSG3_{S317A}$-expressing parasites produced a reproducibly stereotyped immune response (Figures 4A, S8C, and S8D), most notably enriched for the gn33 light chain (after both natural clearance or diminazene treatment) (Figure 4A). These data correlate well with the data observed after VSG2 infections, suggestive of a trend where non-apically glycosylated VSGs elicit stereotyped responses. Again, recombinant expression of a number of these heavy and light chain pairs as secreted IgG1s in 293T cells show that many of the antibodies elicited by $VSG3_{S317A}$ coats are capable of binding their cognate parasites (Figures 4B and 4C); however, non-binders are also present (Figures S9A and S9B).

CellPress
OPEN ACCESS

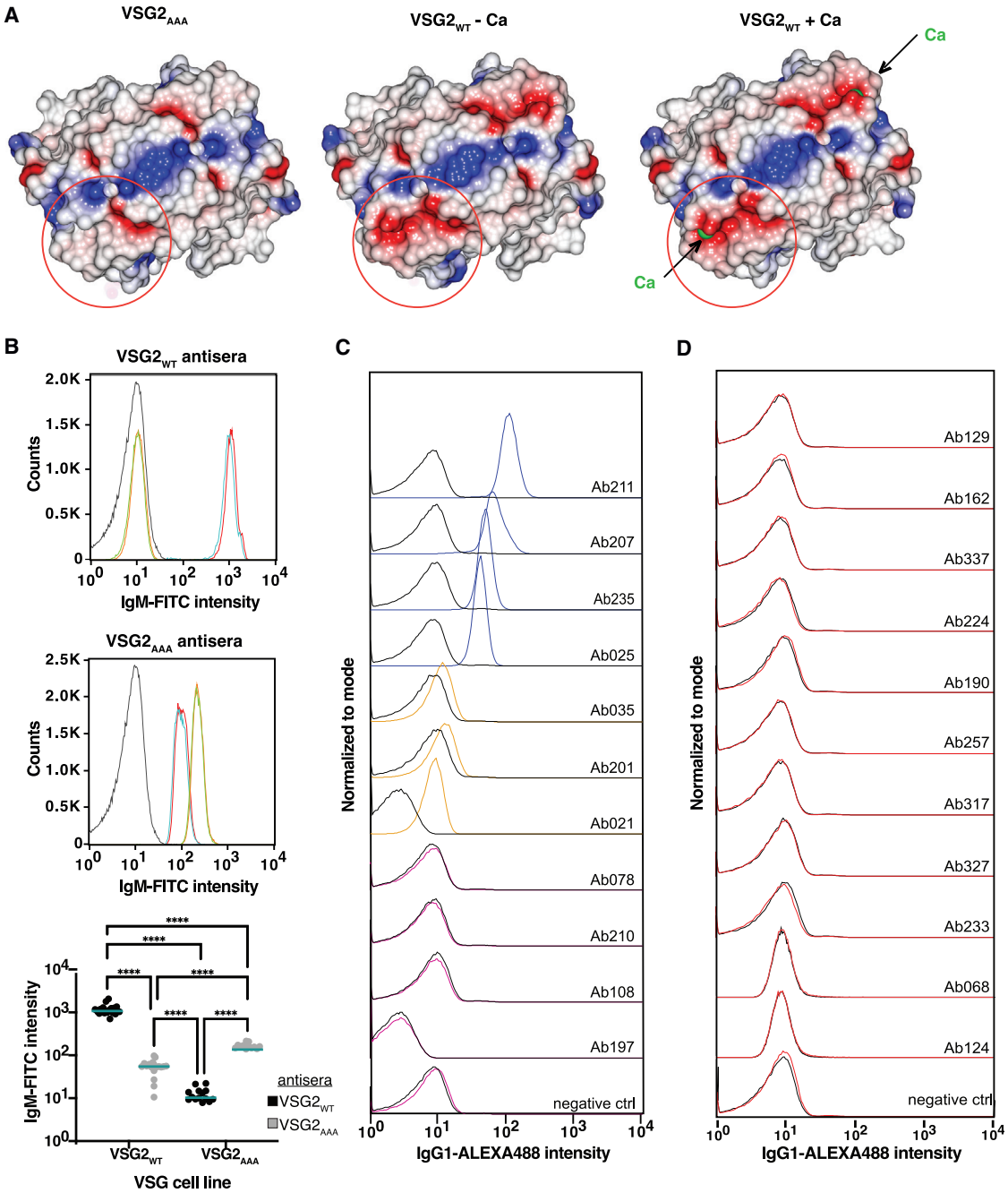

Figure 3. Residues surrounding the calcium binding pocket of $VSG2_{WT}$ define an immunodominant epitope

(A) Molecular surfaces of $VSG2_{WT}$+ calcium (this study), $VSG2_{WT}$− calcium (from Freymann et al.[22]) and $VSG2_{AAA}$. The VSGs are oriented looking "down" on the top lobe of the protein, the orientation rotated 90° about a horizontal axis in comparison to Figure 2A. The surfaces are colored by relative electrostatic potential (blue is basic/positively charged, red is acidic/negatively charged, and white is neutral).

(B) Histograms reflecting binding intensities of antisera collected from mice infected with $VSG2_{WT}$- or $VSG2_{AAA}$-covered parasites (top two panels, respectively) to $VSG2_{WT}$ and $VSG2_{AAA}$ cells (blue and red correspond to two independent clones of $VSG2_{WT}$ parasites; green and orange correspond to two independent clones of $VSG2_{AAA}$ parasites). Unstained cells were used as a negative control (black peaks). Bottom panel shows the median fluorescence intensity (MFI) of the binding of several antisera collected from mice infected with either $VSG2_{WT}$ (black dots, n = 18) or $VSG2_{AAA}$ (gray dots, n = 12) trypanosomes to $VSG2_{WT}$ and $VSG2_{AAA}$ cell lines (x axis). The median for each group is depicted by the teal horizontal lines. MFI values were compared using the Brown-Forsythe and Welch ANOVA tests followed by Dunnett's multiple-comparison test (GraphPad Prism, v.9.3.1). Adjusted p values for all comparisons were calculated to be < 0.0001 (shown as **** in the plot) and considered statistically significant.

(legend continued on next page)

Although the common light chain variable gene (gn33) is clearly important for binding, the proper heavy chain is also necessary, since pairing of the gn33 light chain with a different VH can result in a loss of binding (Figures S9C and S9D). Whether the common light chain plays a role in increasing antibody binding to the repetitive coat remains to be investigated.

As hypothesized, after diminazene-treated $VSG3_{WT}$ infections (the high virulence of the strain is incompatible with natural clearance[15]), we found that the light-chain restriction seen with $VSG3_{S317A}$-elicited repertoires is now entirely abolished, strongly suggesting that the addition of up to three *O*-linked hexoses per VSG3 molecule functions to diversify the presumed immunodominant epitope presented by the $VSG3_{S317A}$-coated parasite (Figure 4D). Furthermore, the addition of sugars entirely prevented the major VL (gn33) carrying antibody pairs of $VSG3_{S317A}$ from binding to $VSG3_{WT}$-coated parasites (Figures 4B and 4C), suggesting that antibodies elicited to the mutant parasite coat are focused near exclusively on the epitope that contains the *O*-linked hexoses. Conversely, of the four antibodies we reconstituted and tested that were elicited by the wild-type ($VSG3_{WT}$) infection, three were able to bind the sugar-less coat, as $VSG3_{WT}$-covered parasites do possess a certain percentage of S317A VSGs on their coat, attributed to the "0 hexose" version of the wild-type protein,[27] and one was selective to the sugar on S317 (capable only of binding the wild type) (Figures 4B and 4C).

The anti-VSG3 repertoire is highly sensitive to a prominent immunodominant epitope on the surface of VSG3

A comparison of mutant and wild-type structures verified that the protein surface between the two VSG3 variants was identical (Figure 5A) but yielded a surprise in the form of an additional sugar in a neighboring serine (S319). We confirmed this in the $VSG3_{WT}$ structure by re-solving it (Figures 5A, 5B, S4B, and S4E; Table S2). S319 is part of the surface-exposed loop harboring S317. In a previous study,[27] both by crystallography and mass spectrometry, glycosylation of S319 was not clearly present, likely due to intrinsic lability of the moiety. However, here we were able to observe strong density for the sugar on S319 in the $VSG3_{WT}$ and $VSG3_{S317A}$ mutant crystal structures, as well as to confirm the presence of hexose groups on S317 and S319 by mass spectrometry (Figure S10). Subsequent determination of the crystal structures of the S319A mutant as well as the double mutant (combining S317A and S319A, or "SSAA") did not reveal any significant structural differences when compared with $VSG3_{WT}$ or $VSG3_{S317A}$ (Figures 5A, 5B, S4B, and S4F–S4H).

Following the experimental protocol that we had used to assess the quality of the repertoires elicited by $VSG3_{WT}$ and $VSG3_{S317A}$, we also generated plasma cell antibody repertoires elicited by $VSG3_{S319A}$ and $VSG3_{SSAA}$ (Figure 5C) and tested those for their ability to bind either their cognate parasites or to cross-react with the wild type and other mutants. We found that $VSG3_{SSAA}$ parasites elicited repertoires very similar to those elicited by the $VSG3_{S317A}$ mutant alone (e.g., dominant presence of the gn33 light chain V gene and 30-60.6.70 or J558.26.116 heavy chain genes), whereas $VSG3_{S319A}$ single mutants elicited broader repertoires that were very similar to those elicited by $VSG3_{WT}$ (no gn33 dominance, for example) (Figure 5C). In turn, this suggests that the $VSG3_{WT}$ repertoire is strongly influenced by the one-to-three hexoses linked to S317,[27] but negligibly by the glycans linked to S319; similarly, that the S317A determined repertoire is indifferent to the presence of the sugar on S319, as the repertoire does not change significantly in the double mutant (corrected p value > 0.05, Table S4).

We then tested recombinant antibodies that were elicited after infection with each of these variants for the ability to cross-react with each of the other variants, we identified four classes of binders:

(1) Antibodies that could bind all four variants (like ab239 or ab222; Figures 6A and 6B); these were elicited by both $VSG3_{WT}$ and $VSG3_{SSAA}$, suggesting that they bind a common peptide epitope at a distance from the epitope-defining sugar.
(2) Antibodies that bound only the epitope-defining sugar-containing variants $VSG3_{WT}$ and $VSG3_{S319A}$ (like ab250; Figures 6A and 6B) but not the other two variants; suggesting that they bind the sugar-containing epitope but not the same epitope without the carbohydrate (and are therefore potentially sugar selective);
(3) Antibodies that bound only the variants that lacked the epitope-defining sugar at S317 ($VSG3_{S317A}$ and $VSG3_{SSAA}$, like ab021), suggesting that they bind the same peptide epitope defined by the sugar but are inhibited by the presence of the sugar in the other two variants.
(4) Finally, antibodies that only bound the $VSG3_{S317A}$ variant (e.g., ab234), potentially suggestive of an additional minor epitope partly defined by the S319 sugar.

We also attempted to crystallize $VSG3_{WT}$ together with $VSG3_{WT}$ Fab fragments. Here, we were able to co-purify Fabs (e.g., Fab239 with an IgG2a original isotype), using gel filtration chromatography (Figures S3C and S3D); but, similarly to the attempts with $VSG2_{WT}$ and its cognate antibodies, we did not manage to obtain co-crystals.

These results underscore the immunodominance of the relevant epitopes and the exquisite discrimination of the resulting antibodies. Specifically, they suggest that the immunodominant epitope that characterizes the $VSG3_{WT}$ coat is limited to the immediate amino acids surrounding the S317-*O*-glucose (including that sugar but excluding its companion on S319).

(C) Histograms reflecting binding intensities of the antibodies presented in Figure 1D with wild-type parasites (in different colors) and AAA-mutant parasites (black). Different colors are meant to distinguish differential binding intensity: purple, no binding; mustard, poor binding; blue, good binding. Staining with supernatants from untransfected cells (no plasmid) is used as a negative control. All data are normalized to mode. The gating strategy is shown in Figure S1C.
(D) Histograms showing binding intensities of recombinant antibodies with wild-type parasites (red) and AAA-mutant parasites (black). All other parameters are the same as for (C).

CellPress
OPEN ACCESS

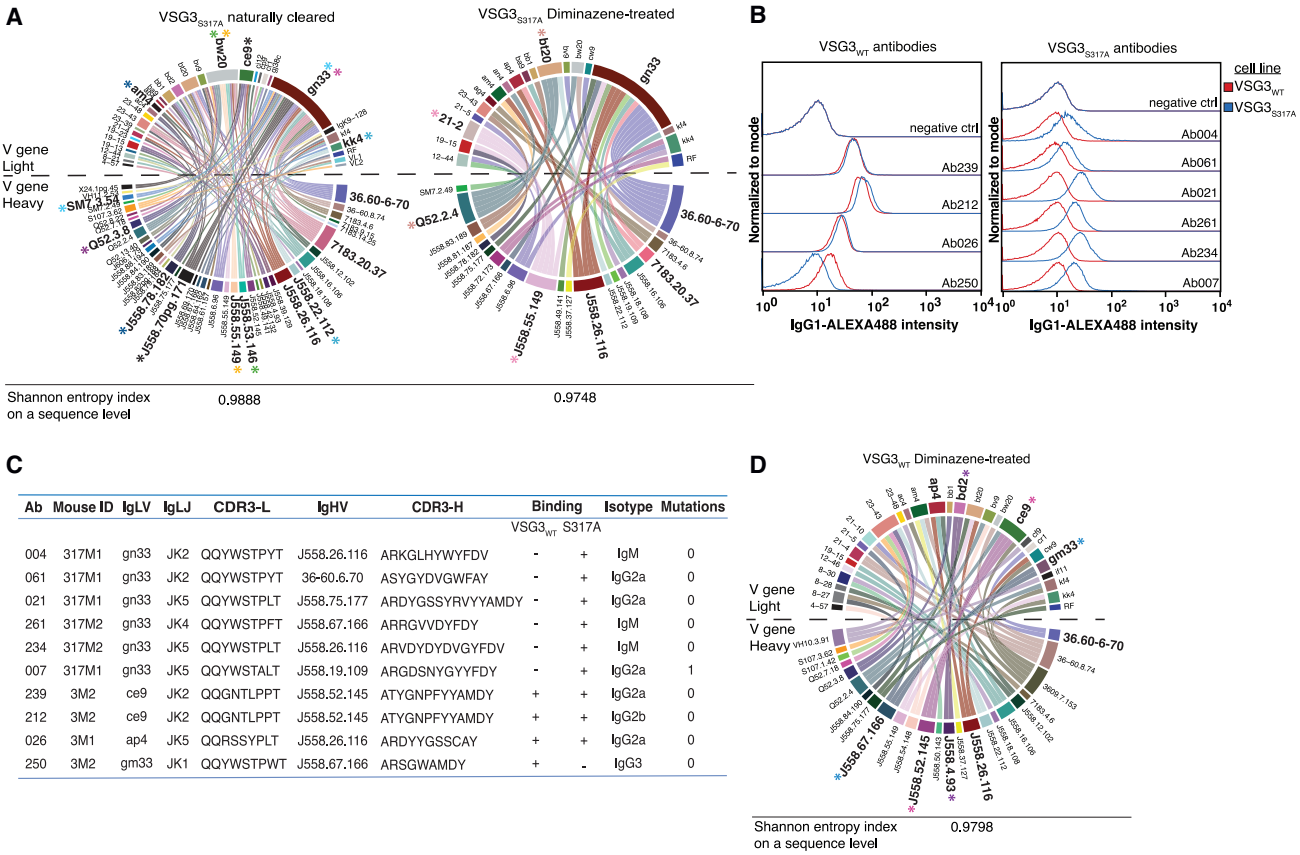

Ab	Mouse ID	IgLV	IgLJ	CDR3-L	IgHV	CDR3-H	Binding VSG3$_{WT}$	Binding S317A	Isotype	Mutations
004	317M1	gn33	JK2	QQYWSTPYT	J558.26.116	ARKGLHYWYFDV	-	+	IgM	0
061	317M1	gn33	JK2	QQYWSTPYT	36-60.6.70	ASYGYDVGWFAY	-	+	IgG2a	0
021	317M1	gn33	JK5	QQYWSTPLT	J558.75.177	ARDYGSSYRVYYAMDY	-	+	IgG2a	0
261	317M2	gn33	JK4	QQYWSTPFT	J558.67.166	ARRGVVDYFDY	-	+	IgM	0
234	317M2	gn33	JK5	QQYWSTPLT	J558.26.116	ARVDYDYDVGYFDV	-	+	IgM	0
007	317M1	gn33	JK5	QQYWSTALT	J558.19.109	ARGDSNYGYYFDY	-	+	IgG2a	1
239	3M2	ce9	JK2	QQGNTLPPT	J558.52.145	ATYGNPFYYAMDY	+	+	IgG2a	0
212	3M2	ce9	JK2	QQGNTLPPT	J558.52.145	ATYGNPFYYAMDY	+	+	IgG2b	0
026	3M1	ap4	JK5	QQRSSYPLT	J558.26.116	ARDYYGSSCAY	+	+	IgG2a	0
250	3M2	gm33	JK1	QQYWSTPWT	J558.67.166	ARSGWAMDY	+	-	IgG3	0

Figure 4. VSG3$_{S317A}$ parasites elicit a restricted B cell response, with preferential utilization of a light chain V$_{\kappa}$ gene (gn33)

(A) Circos diagrams generated for the VSG3$_{S317A}$ V gene signatures of four mice infections (n = 4), two naturally cleared (left, n = 113 pairs) and two diminazene treated (right, n = 49 pairs). Different colors depict each heavy chain variable gene (bottom half of the plot), and each light chain variable gene (top half of the plot). The heavy and light chain variable gene pairings that form the antibodies are illustrated as connector lines starting from the heavy chain genes, providing also information about the frequency of the pairings. Genes from both chains that appeared only once and resulted in single heavy-light pairings, were considered background and were removed from the plot. Colored asterisks depict individual B cells that correspond to clones (i.e., share the same V heavy and V light gene segments but also the same DJ or J genes and the same CDR3 length and sequence). Shannon entropy shows clonal diversity on a sequence level, a number of 1.0 shows 100% clonal diversity (no clones), while a value of 0.0 corresponds to 0% clonal diversity (only clones).

(B) Left: FACS analysis of heavy and light chain pairs selected from the VSG3$_{WT}$ repertoire, produced recombinantly as IgG1 antibodies. The plots depict antibody binding to VSG3$_{WT}$ (red) or VSG3$_{S317A}$ (blue) *T. brucei* cells. Parasites were first stained with each antibody supernatant, and then with (mouse anti-human) AlexaFluor488-IgG1 secondary antibody. The gating strategy is shown in Figure S1C. Staining with supernatants from untransfected cells (no plasmid) serves as a negative control. All data are normalized to mode. Right: FACS showing the same experimental setup but now for binding of recombinant antibodies selected from the VSG3$_{S317A}$ repertoire.

(C) Table of all the VSG3$_{S317A}$ antibodies with gn33 as a light chain that bound to the cognate and WT cells, as well as of all the VSG3$_{WT}$ antibodies and their binding to cognate and mutant cells. The (+) symbol indicates binding while the (−) lack of binding. V and J segments as well as the CDR3 of both heavy and light chain genes are shown, along with the binding to the respective parasites. The original antibody isotype, as well as somatic hypermutations, if any, are also shown.

(D) Circos plots generated for the VSG3$_{WT}$ V gene signatures from two mice (n = 2) whose infections were treated with diminazene (n = 53 pairs), as described in (A).

DISCUSSION

The antibody-mediated interactions between host and trypanosomes have been intensively studied over the years but remain poorly understood. Investigating immune responses against the coat of the trypanosomes, together with the cognate VSG structures, will provide greater insights into the nature of such interactions. Here, we show that mouse infection with trypanosomes of a specific VSG coat leads to robust plasma cell expansion comprised of cells that are remarkably restricted in their antibody repertoire. This restriction of chain usage allowed us to use n = 2 mice per repertoire (something already reported in the literature[29,30]), complemented by the fact that both diminazene and naturally cleared infections of the same VSG (n = 4 in this case) showed similar chain dominance in the repertoires (Figures 1C and 4A).

The aforementioned plasma cell expansion is reminiscent of acute infection with Dengue in humans.[31] It is important to note, however, that repertoires elicited by Dengue are hypermutated and show a high degree of clonality, suggesting prior

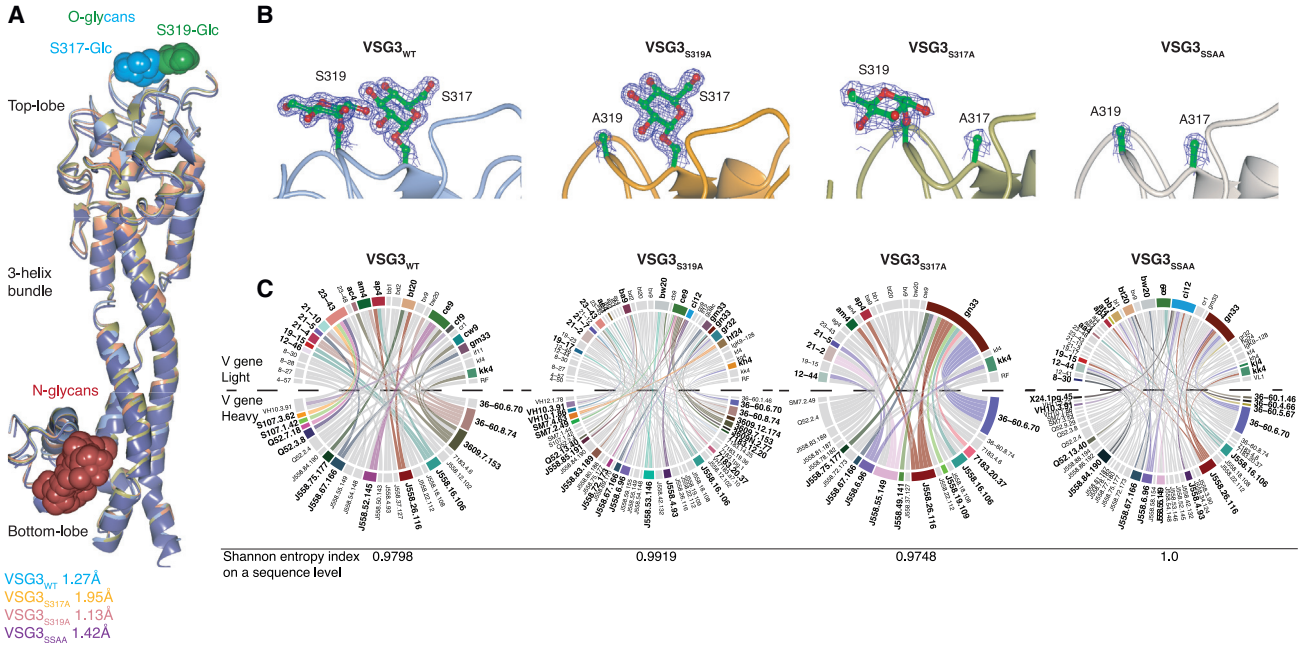

Figure 5. Nearly identical VSG3 variant coats elicit distinct V gene signatures

(A) Overlaid crystal structures of all four VSG3 monomers, shown as ribbon diagrams and colored in blue (WT), gold (S317A), salmon (S319A), and purple (SSAA). The N-glycans are represented as red spheres on the bottom lobe, while the *O*-linked sugars as blue (S317-sugar) and green (S319-sugar) spheres on the top lobe.

(B) Electron density maps (2Fo-Fc, contoured at 1σ) focused on the presence or absence of the S317 and S319 *O*-glucose molecules for all individual proteins as indicated by the labeling.

(C) Circos plots of the diminazene-treated plasma cell antibody repertoires (V signatures shown only) of WT (n = 53 pairs, n = 2 mice), S317A (n = 49 pairs, n = 2 mice), S319A (n = 108 pairs, n = 2 mice), and SSAA (n = 102 pairs, n = 2 mice). Different colors depict each heavy chain variable gene (bottom half of the plot), and each light chain variable gene (top half of the plot). The heavy and light chain variable gene pairings that form the antibodies are illustrated as connector lines starting from the heavy chain genes, providing also information about the frequency of the pairings. Genes from both chains that appeared only once and resulted in single heavy-light pairings were considered background and were removed from the plot. The antibody pairs picked for validation are presented in color, while all other genes are in gray. Shannon entropy shows clonal diversity on a sequence level (a value of 1.0 shows 100% clonal diversity [no clones], while a value of 0.0 corresponds to 0% clonal diversity [only clones]).

exposure. In contrast, repertoires elicited by VSGs are essentially unmutated (Figures 4C and 6B). Furthermore, although each VSG protein appears to elicit a distinct V gene signature, the antibodies characterized by this signature are not clonal (i.e., they contain different D and J segments and consequently different CDR3 sequences). Although the existence of a robust serological response to trypanosome infection has been recognized for years (most recently by Verdi et al.[1]) our work confirms that this response is polyclonal.[11] Such polyclonal antibodies have been documented in other infections as well, e.g., influenza,[32–34] dengue,[31,35] hepatitis C,[36] and HIV.[37] Our work extends these findings by demonstrating that this polyclonal response is highly stereotyped between animals (Figures S2 and S8), is VSG specific, and is repertoire restricted.

The usage of distinct V gene signatures per VSG-elicited repertoire, which is highly reproducible between mice, implies the existence of common paratopes. In turn, this suggests that each VSG contains a small cohort of immunodominant epitopes to which the common paratopes might map. To date, co-crystal structures of VSGs and cognate antibodies are not available, and thus a definitive assignment of antibody-bound epitopes cannot be made. However, mutations in structurally defined features of each VSG can lead to loss of antibody binding, suggesting that key immunodominant epitopes reside within a tightly circumscribed region of each VSG. For VSG2, such a feature is the calcium binding pocket, identified on the top lobe of the molecule: disruption of the pocket by point mutations in the calcium-coordinating residues (DND) did not lead to structural alteration but did result in loss of recognition by $VSG2_{WT}$-elicited antisera and monoclonal antibodies. This implies that the subdomain of $VSG2_{WT}$ that contains the DND motif forms an epitope that dominates the antibody response against this specific coat.

Similarly, for VSG3, an immunodominant epitope is defined by a small region surrounding the *O*-linked glucose on serine 317. Previous work had shown that this particular hexose anchors a chain of up to three additional hexoses to S317, leading Pinger et al. to hypothesize that hexose heterogeneity contributed to repertoire diversification that would be detrimental to the immune response against the organism.[27] Indeed, we found that infections with $VSG3_{S317A}$-coated trypanosomes elicited restricted antibody repertoires with a VL gene signature dominated by VL-gn33, but that this signature disappeared after infection with the wild-type VSG3 strain. This loss of signature correlates with increased virulence: infection with $VSG3_{S317A}$-coated

CellPress
OPEN ACCESS

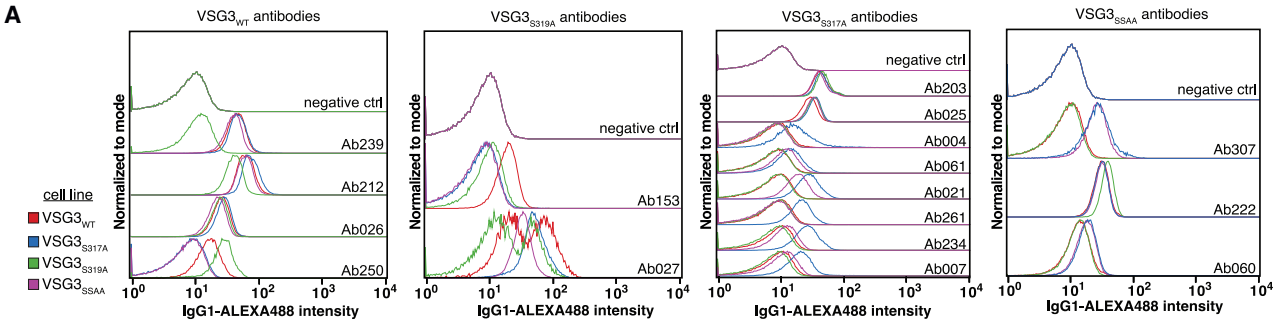

B

Ab	Mouse ID	IgLV	IgLJ	CDR3-L	IgHV	CDR3-H	Binding				Isotype	Mutations
							$VSG3_{WT}$	S317A	S319A	SSAA		
234	317M2	gn33	JK5	QQYWSTPLT	J558.26.116	ARVDYDYDVGYFDV	-	+	-	-	IgM	0
021	317M1	gn33	JK5	QQYWSTPLT	J558.75.177	ARDYGSSYRVYYAMDY	-	+	-	+	IgG2a	0
250	3M2	gm33	JK1	QQYWSTPWT	J558.67.166	ARSGWAMDY	+	-	+	-	IgG3	0
222	SAM2	aa4	JK2	QQYHSYPPT	J558.16.106	ARLFYYGSSPYFDY	+	+	+	+	IgM	0
239	3M2	ce9	JK2	QQGNTLPPT	J558.52.145	ATYGNPFYYAMDY	+	+	+	+	IgG2a	0

Figure 6. Antibodies elicited by VSG3 variants fall into four classes based on their antigen binding capacity

(A) FACS data showing the binding of the validated antibodies, secreted as IgG1s, to $VSG3_{WT}$ (red)-, $VSG3_{S317A}$ (blue)-, $VSG3_{S319A}$ (green)-, and $VSG3_{SSAA}$ (purple)-covered trypanosomes. Parasites were first stained with each antibody supernatant, followed by staining with a (mouse anti-human) AlexaFluor488-IgG1 secondary antibody. The gating strategy is shown in Figure S1C. Staining with supernatants from untransfected cells (no plasmid) is used as a negative control. All data were normalized to mode.

(B) Table of representative binding patterns of the produced antibodies (also in Figures 4B and 4C) to different trypanosome cell lines. The (+) symbol indicates binding while the (−) indicates non-binding. V and J segments as well as the CDR3 of both heavy and light are shown, along with the binding to the individual cell lines. The original isotypes and somatic hypermutations, if any, are also listed.

trypanosomes is naturally cleared while infection with the wild type is lethal.[15] Perhaps equally interesting is the finding that a second hexose at a neighboring residue to S317 (S319) plays at most a minor role in defining the repertoire, as mutating S319 to alanine resulted in a repertoire that matched the repertoire elicited by the wild-type VSG3 strain (Figure 5C). The lack of substantial impact on the repertoire could be attributed to the unstable nature of the specific sugar even *in vivo*, which is possibly the reason that it was not identified previously (vs., e.g., technical issues to do with cleavage during long-term storage, or even buffer conditions, etc.).[27] However, one class of the antibodies we identified (noted as "binder class"[4]) could potentially bind to epitopes partially defined by the presence of the S319 sugar, as the same antibodies are not able to bind to the double mutant version. Furthermore, mutating both serines resulted in a repertoire matching that elicited by the $VSG3_{S317A}$ mutant (Figure 5C). These findings illustrate the immunodominance of key epitopes on $VSG3_{WT}$, which may be limited to the amino acids in the immediate vicinity of the *O*-glycan on S317, and suggest that the antibody repertoires elicited to specific VSGs not only respond to defined immunodominant features within each VSG but are highly discriminatory as they do so.

Overall, by examining two distinct VSGs and variants thereof, we demonstrate that the antibody response that mediates clearance to a given *T. brucei* coat can be hyperfocused to a restricted set of immunodominant epitopes that are surface exposed. Consequently, the immune response elicited by each *T. brucei* variant coat has the potential to be highly restricted and likely mediated by paratopes within the germline V regions of antibody genes. How *T. brucei* achieves this "immunofocusing" is likely related to the highly dense, repetitive and patterned nature of its surface coat. We hypothesize that this extreme focusing allows the parasite to use short-tract gene conversion or even point mutations (collectively referred to as mosaic formation[3,38]) to expand its antigenicity well beyond what is encoded in its considerable genomic archive. By ensuring that cross-reactivity between coat-defined epitopes will be exceedingly rare, even within similar variants, immunofocusing helps the parasite to perpetually evade the immune response.

Limitations of the study

In this work, we have isolated day-8 post-infection antibodies against different VSGs without a FACS-based baiting step. Even though these are indeed relevant to the host-pathogen interaction, given the behavior of *T. brucei* in the host (with each infection cycle taking about 7–8 days), they are of low affinity. This has limited our ability to assess individual antibody characteristics and has led to the identification of a plethora of what appear to be "non-binders" when expressed in an IgG form, which gives the potentially false impression that a large percentage of the elicited repertoire does not bind antigen. In the future, baited repertoires could be analyzed in combination with expressing the antibodies as their original isotype, IgM (thus with dramatically enhanced avidity), rather than IgG, after extensive optimization of both techniques. In addition (and likely also driven by the low affinities), we were not able to identify any exact

epitopes by crystallography, but rather predict them based on the elicited repertoires and crystal structures.

STAR★METHODS

Detailed methods are provided in the online version of this paper and include the following:

- KEY RESOURCES TABLE
- RESOURCE AVAILABILITY
  - Lead contact
  - Materials availability
  - Data and code availability
- EXPERIMENTAL MODEL AND SUBJECT DETAILS
  - Trypanosome cell lines
  - HEK 293T and 293F cell lines
  - Mouse strains
  - Bacteria
- METHOD DETAILS
  - Plasmids used to generate isogenic *T. brucei* clones
  - *T. brucei* transfections and verification
  - Spleen and antisera collection
  - Flow cytometry and single cell sorting
  - Antibody repertoires and production of antibodies
  - Fab cloning, expression and purification
  - Shannon entropy index calculation
  - VSG purification
  - Crystallization and structural determination
  - Mass spectrometry
  - Isothermal titration calorimetry
- QUANTIFICATION AND STATISTICAL ANALYSIS

SUPPLEMENTAL INFORMATION

Supplemental information can be found online at https://doi.org/10.1016/j.celrep.2023.112262.

ACKNOWLEDGMENTS

We acknowledge synchrotron time at the Paul Scherrer Institut, Villigen, Switzerland (SLS, beamline X06DA, Vincent Olieric and colleagues), the Diamond Light Source (DLS, beamline i03, Neil Paterson and colleagues), and the Advanced Photon Source, Argonne National Laboratory (APS, beamline 24-ID-C, Jonathan P. Schuermann and colleagues). We thank Johan P. Zeelen for assistance with the synchrotron data acquisition and advice in structural determination and Hedda Wardemann for assistance with B cell repertoire analyses and fruitful discussions especially during manuscript revision. Work in the F.N.P. and C.E.S. labs is funded by the Helderleigh Foundation. P.D.B.O. and B.T.C. are funded by the National Institutes of Health P41 GM109824 and P41 GM103314 (to B.T.C.). R.B. and T.R. are supported by the German Research Foundation to T.R. (Ru 747/1-1) within the framework of FOR 2509.

AUTHOR CONTRIBUTIONS

Conceptualization, resources, and funding acquisition, F.N.P. and C.E.S.; investigation, A.G., F.A.-B., G.T., E.P.V., M.L., M.v.S., and C.E.S.; mass spectrometry (MS) analysis, P.D.B.O., B.T.C., R.B., and T.R.; ITC analysis, K.P.; formal analysis, A.G., F.A.-B., C.E.S., P.D.B.O. (MS), B.T.C. (MS), K.P. (ITC), R.B. (MS), and T.R. (MS); visualization, A.G., F.A.-B., C.E.S., P.D.B.O. (MS), B.T.C. (MS), K.P. (ITC), R.B. (MS), and T.R. (MS); writing – original draft, F.N.P. and C.E.S.; writing – review & editing, F.N.P., C.E.S., A.G., F.A.-B., G.T., and J.P.V.

DECLARATION OF INTERESTS

F.N.P., C.E.S., and J.P.V. report being shareholders of Panosome GmbH. F.N.P. and C.E.S. report being the managing directors of Panosome GmbH.

Received: June 9, 2022
Revised: December 2, 2022
Accepted: February 28, 2023

REFERENCES

1. Verdi, J., Zipkin, R., Hillman, E., Gertsch, R.A., Pangburn, S.J., Thomson, R., Papavasiliou, N., Sternberg, J., and Raper, J. (2020). Inducible germline IgMs bridge trypanosome lytic factor assembly and parasite recognition. Cell Host Microbe *28*, 79–88.e4. https://doi.org/10.1016/j.chom.2020.04.012.
2. Stijlemans, B., Radwanska, M., De Trez, C., and Magez, S. (2017). African trypanosomes undermine humoral responses and vaccine development: link with inflammatory responses? Front. Immunol. *8*, 582. https://doi.org/10.3389/fimmu.2017.00582.
3. Mugnier, M.R., Cross, G.A.M., and Papavasiliou, F.N. (2015). The in vivo dynamics of antigenic variation in Trypanosoma brucei. Science *347*, 1470–1473. https://doi.org/10.1126/science.aaa4502.
4. Grünfelder, C.G., Engstler, M., Weise, F., Schwarz, H., Stierhof, Y.-D., Boshart, M., and Overath, P. (2002). Accumulation of a GPI-anchored protein at the cell surface requires sorting at multiple intracellular levels. Traffic *3*, 547–559.
5. Aresta-Branco, F., Erben, E., Papavasiliou, F.N., and Stebbins, C.E. (2019). Mechanistic similarities between antigenic variation and antibody diversification during trypanosoma brucei infection. Trends Parasitol. *35*, 302–315. https://doi.org/10.1016/j.pt.2019.01.011.
6. Bangs, J.D. (2018). Evolution of antigenic variation in african trypanosomes: variant surface glycoprotein expression, structure, and function. Bioessays *40*, e1800181. https://doi.org/10.1002/bies.201800181.
7. Zoll, S., Lane-Serff, H., Mehmood, S., Schneider, J., Robinson, C.v., Carrington, M., and Higgins, M.K. (2018). The structure of serum resistance-associated protein and its implications for human African trypanosomiasis. Nat. Microbiol. *3*, 295–301. https://doi.org/10.1038/s41564-017-0085-3.
8. Hempelmann, A., Hartleb, L., van Straaten, M., Hashemi, H., Zeelen, J.P., Bongers, K., Papavasiliou, F.N., Engstler, M., Stebbins, C.E., and Jones, N.G. (2021). Nanobody-mediated macromolecular crowding induces membrane fission and remodeling in the African trypanosome. Cell Rep. *37*, 109923. https://doi.org/10.1016/j.celrep.2021.109923.
9. Silva-Barrios, S., Charpentier, T., and Stäger, S. (2018). The deadly dance of B cells with trypanosomatids. Trends Parasitol. *34*, 155–171. https://doi.org/10.1016/j.pt.2017.10.001.
10. Morrison, L.J., Majiwa, P., Read, A.F., and Barry, J.D. (2005). Probabilistic order in antigenic variation of Trypanosoma brucei. Int. J. Parasitol. *35*, 961–972. https://doi.org/10.1016/j.ijpara.2005.05.004.
11. Müller, N., Mansfield, J.M., and Seebeck, T. (1996). Trypanosome variant surface glycoproteins are recognized by self-reactive antibodies in uninfected hosts. Infect. Immun. *64*, 4593–4597.
12. Diffley, P. (1983). Trypanosomal surface coat variant antigen causes polyclonal lymphocyte activation. J. Immunol. *131*, 1983–1986.
13. Campbell, G.H., Esser, K.M., and Weinbaum, F.I. (1977). Trypanosoma rhodesiense infection in B-Cell-Deficient mice. Infect. Immun. *18*, 434–438.
14. Carrington, M., Miller, N., Blum, M., Roditi, I., Wiley, D., and Turner, M. (1991). Variant specific glycoprotein of trypanosoma brucei consists of

two domains each having an independently conserved pattern of cysteine residues. J. Mol. Biol. *221*, 823–835.

15. Pinger, J., Chowdhury, S., and Papavasiliou, F.N. (2017). Variant surface glycoprotein density defines an immune evasion threshold for African trypanosomes undergoing antigenic variation. Nat. Commun. *8*, 828. https://doi.org/10.1038/s41467-017-00959-w.
16. Black, S.J., Sendashonga, C.N., O'brien, C., Borowy, N.K., Naessens, M., Webster, P., and Murray, M. (1985). Regulation of parasitaemia in mice infected with trypanosoma brucei. In The Biology of Trypanosomes. Current Topics in Microbiology and Immunology, L. Hudson, ed., pp. 93–118. https://doi.org/10.1007/978-3-642-70538-0_5.
17. Jayaraman, S., Harris, C., Paxton, E., Donachie, A.M., Vaikkinen, H., McCulloch, R., Hall, J.P.J., Kenny, J., Lenzi, L., Hertz-Fowler, C., et al. (2019). Application of long read sequencing to determine expressed antigen diversity in Trypanosoma brucei infections. PLoS Neglected Trop. Dis. *13*, e0007262. https://doi.org/10.1371/journal.pntd.0007262.
18. Tiller, T., Meffre, E., Yurasov, S., Tsuiji, M., Nussenzweig, M.C., and Wardemann, H. (2008). Efficient generation of monoclonal antibodies from single human B cells by single cell RT-PCR and expression vector cloning. J. Immunol. Methods *329*, 112–124. https://doi.org/10.1016/j.jim.2007.09.017.
19. Scheid, J.F., Mouquet, H., Feldhahn, N., Walker, B.D., Pereyra, F., Cutrell, E., Seaman, M.S., Mascola, J.R., Wyatt, R.T., Wardemann, H., and Nussenzweig, M.C. (2009). A method for identification of HIV gp140 binding memory B cells in human blood. J. Immunol. Methods *343*, 65–67. https://doi.org/10.1016/j.jim.2008.11.012.
20. Pracht, K., Meinzinger, J., Daum, P., Schulz, S.R., Reimer, D., Hauke, M., Roth, E., Mielenz, D., Berek, C., Côrte-Real, J., et al. (2017). A new staining protocol for detection of murine antibody-secreting plasma cell subsets by flow cytometry. Eur. J. Immunol. *47*, 1389–1392. https://doi.org/10.1002/eji.201747019.
21. Triller, G., Scally, S.W., Costa, G., Pissarev, M., Kreschel, C., Bosch, A., Marois, E., Sack, B.K., Murugan, R., Salman, A.M., et al. (2017). Natural parasite exposure induces protective human anti-malarial antibodies. Immunity *47*, 1197–1209.e10. https://doi.org/10.1016/j.immuni.2017.11.007.
22. Freymann, D., Down, J., Carrington, M., Roditi, I., Turner, M., and Wiley, D. (1990). 2.9 A resolution structure of the N-terminal domain of a variant surface glycoprotein from trypanosoma brucei. J. Mol. Biol. *216*, 141–160.
23. Metcalf, P., Blum, M., Freymann, D., Turner, M., and Wiley, D.C. (1987). Two Variant Surface Glycoproteins of Trypanosoma brucei of different sequence classes have similar 6A resolution X-ray structures. Nature *325*, 84–86. https://doi.org/10.1038/325084a0.
24. Cross, G.A. (1975). Identification, purification and properties of clone-specific glycoprotein antigens constituting the surface coat of Trypanosoma brucei. Parasitology *71*, 393–417. https://doi.org/10.1017/S003118200004717X.
25. Cross, G.A. (1984). Release and purification of trypanosoma brucei variant surface glycoprotein. J. Cell. Biochem. *24*, 79–90. https://doi.org/10.1002/jcb.240240107.
26. Holm, L. (2020). DALI and the persistence of protein shape. Protein Sci. *29*, 128–140. https://doi.org/10.1002/pro.3749.
27. Pinger, J., Nešić, D., Ali, L., Aresta-Branco, F., Lilic, M., Chowdhury, S., Kim, H.S., Verdi, J., Raper, J., Ferguson, M.A.J., et al. (2018). African trypanosomes evade immune clearance by O-glycosylation of the VSG surface coat. Nat. Microbiol. *3*, 932–938. https://doi.org/10.1038/s41564-018-0187-6.
28. Lisowska, E. (2002). The role of glycosylation in protein antigenic properties. Cell. Mol. Life Sci. *59*, 445–455.
29. Goldstein, L.D., Chen, Y.J.J., Wu, J., Chaudhuri, S., Hsiao, Y.C., Schneider, K., Hoi, K.H., Lin, Z., Guerrero, S., Jaiswal, B.S., et al. (2019). Massively parallel single-cell B-cell receptor sequencing enables rapid discovery of diverse antigen-reactive antibodies. Commun. Biol. *2*, 304. https://doi.org/10.1038/s42003-019-0551-y.
30. Khass, M., Buckley, K., Kapoor, P., Schelonka, R.L., Watkins, L.S., Zhuang, Y., and Schroeder, H.W. (2013). Recirculating bone marrow B cells in C57BL/6 mice are more tolerant of highly hydrophobic and highly charged CDR-H3s than those in BALB/c mice. Eur. J. Immunol. *43*, 629–640. https://doi.org/10.1002/eji.201242936.
31. Waickman, A.T., Gromowski, G.D., Rutvisuttinunt, W., Li, T., Siegfried, H., Victor, K., Kuklis, C., Gomootsukavadee, M., McCracken, M.K., Gabriel, B., et al. (2020). Transcriptional and clonal characterization of B cell plasmablast diversity following primary and secondary natural DENV infection. EBioMedicine *54*, 102733. https://doi.org/10.1016/j.ebiom.2020.102733.
32. Lee, J., Paparoditis, P., Horton, A.P., Frühwirth, A., McDaniel, J.R., Jung, J., Boutz, D.R., Hussein, D.A., Tanno, Y., Pappas, L., et al. (2019). Persistent antibody clonotypes dominate the serum response to influenza over multiple years and repeated vaccinations. Cell Host Microbe *25*, 367–376.e5. https://doi.org/10.1016/j.chom.2019.01.010.
33. Woods, A., Monneaux, F., Soulas-Sprauel, P., Muller, S., Martin, T., Korganow, A.-S., and Pasquali, J.-L. (2007). Influenza virus-induced type I interferon leads to polyclonal B-cell activation but does not break down B-cell tolerance. J. Virol. *81*, 12525–12534. https://doi.org/10.1128/jvi.00839-07.
34. Lee, J., Boutz, D.R., Chromikova, V., Joyce, M.G., Vollmers, C., Leung, K., Horton, A.P., DeKosky, B.J., Lee, C.H., Lavinder, J.J., et al. (2016). Molecular-level analysis of the serum antibody repertoire in young adults before and after seasonal influenza vaccination. Nat. Med. *22*, 1456–1464. https://doi.org/10.1038/nm.4224.
35. Correa, A.R.V., Berbel, A.C.E.R., Papa, M.P., Morais, A.T.S.d., Peçanha, L.M.T., and Arruda, L.B.d. (2015). Dengue virus directly stimulates Polyclonal B cell activation. PLoS One *10*, e0143391. https://doi.org/10.1371/journal.pone.0143391.
36. de Vita, S., Quartuccio, L., and Fabris, M. (2008). Hepatitis C virus infection, mixed cryoglobulinemia and BLyS upregulation: targeting the infectious trigger, the autoimmune response, or both? Autoimmun. Rev. *8*, 95–99. https://doi.org/10.1016/j.autrev.2008.05.005.
37. Moir, S., and Fauci, A.S. (2009). B cells in HIV infection and disease. Nat. Rev. Immunol. *9*, 235–245. https://doi.org/10.1038/nri2524.
38. Hall, J.P.J., Wang, H., and Barry, J.D. (2013). Mosaic VSGs and the scale of trypanosoma brucei antigenic variation. PLoS Pathog. *9*, e1003502. https://doi.org/10.1371/journal.ppat.1003502.
39. Alsford, S., Kawahara, T., Glover, L., and Horn, D. (2005). Tagging a T. brucei RRNA locus improves stable transfection efficiency and circumvents inducible expression position effects. Mol. Biochem. Parasitol. *144*, 142–148. https://doi.org/10.1016/j.molbiopara.2005.08.009.
40. Adams, P.D., Afonine, P.v., Bunkóczi, G., Chen, V.B., Davis, I.W., Echols, N., Headd, J.J., Hung, L.W., Kapral, G.J., Grosse-Kunstleve, R.W., et al. (2010). PHENIX: a comprehensive Python-based system for macromolecular structure solution. Acta Crystallogr. D Biol. Crystallogr. *66*, 213–221. https://doi.org/10.1107/S0907444909052925.
41. Emsley, P., Lohkamp, B., Scott, W.G., and Cowtan, K. (2010). Features and development of coot. Acta Crystallogr. D Biol. Crystallogr. *66*, 486–501. https://doi.org/10.1107/S0907444910007493.
42. Pettersen, E.F., Goddard, T.D., Huang, C.C., Meng, E.C., Couch, G.S., Croll, T.I., Morris, J.H., and Ferrin, T.E. (2021). UCSF ChimeraX: structure visualization for researchers, educators, and developers. Protein Sci. *30*, 70–82. https://doi.org/10.1002/pro.3943.
43. Hirumi, H., and Hirumi, K. (1989). Continuous cultivation of trypanosoma brucei blood stream forms in a medium containing a low concentration of serum protein without feeder cell layers. J. Parasitol. *75*, 985–989.
44. Burkard, G., Fragoso, C.M., and Roditi, I. (2007). Highly efficient stable transformation of bloodstream forms of Trypanosoma brucei. Mol. Biochem. Parasitol. *153*, 220–223. https://doi.org/10.1016/j.molbiopara.2007.02.008.

45. Ye, J., Ma, N., Madden, T.L., and Ostell, J.M. (2013). IgBLAST: an immunoglobulin variable domain sequence analysis tool. Nucleic Acids Res. *41*, W34–W40. https://doi.org/10.1093/nar/gkt382.

46. Olinares, P.D.B., and Chait, B.T. (2020). Native mass spectrometry analysis of affinity-captured endogenous yeast RNA exosome complexes. In The Eukaryotic RNA Exosome, Methods and Protocols Methods in Molecular Biology (Clifton, N.J.), pp. 357–382.

47. Reid, D.J., Diesing, J.M., Miller, M.A., Perry, S.M., Wales, J.A., Montfort, W.R., and Marty, M.T. (2019). MetaUniDec: high-throughput deconvolution of native mass spectra. J. Am. Soc. Mass Spectrom. *30*, 118–127. https://doi.org/10.1007/s13361-018-1951-9.

48. Marty, M.T., Baldwin, A.J., Marklund, E.G., Hochberg, G.K.A., Benesch, J.L.P., and Robinson, C.v. (2015). Bayesian deconvolution of mass and ion mobility spectra: from binary interactions to polydisperse ensembles. Anal. Chem. *87*, 4370–4376. https://doi.org/10.1021/acs.analchem.5b00140.

49. Zamze, S.E., Ashford, D.A., Wooten, E.W., Rademacher, T.W., and Dwek, R.A. (1991). Structural characterization of the asparagine-linked oligosaccharides from Trypanosoma brucei Type II and Type III variant surface glycoproteins. J. Biol. Chem. *266*, 20244–20261. https://doi.org/10.1016/s0021-9258(18)54916-4.

50. Mehlert, A., Richardson, J.M., and Ferguson, M.A. (1998). Structure of the glycosylphosphatidylinositol membrane anchor glycan of a class-2 variant surface glycoprotein from trypanosoma brucei. J. Mol. Biol. *277*, 379–392.

51. Manthri, S., Güther, M.L.S., Izquierdo, L., Acosta-serrano, A., and Ferguson, M.A.J. (2008). Deletion of the TbALG3 gene demonstrates site-specific N-glycosylation and N-glycan processing in Trypanosoma brucei. Glycobiology *18*, 367–383. https://doi.org/10.1093/glycob/cwn014.

52. Fecher-Trost, C., Wissenbach, U., Beck, A., Schalkowsky, P., Stoerger, C., Doerr, J., Dembek, A., Simon-Thomas, M., Weber, A., Wollenberg, P., et al. (2013). The in vivo TRPV6 protein starts at a non-AUG triplet, decoded as methionine, upstream of canonical initiation at AUG. J. Biol. Chem. *288*, 16629–16644. https://doi.org/10.1074/jbc.M113.469726.

CellPress
OPEN ACCESS

STAR★METHODS

KEY RESOURCES TABLE

REAGENT or RESOURCE	SOURCE	IDENTIFIER
Antibodies		
anti-VSG2	Lab internal	Pinger et al.[15]; PMID: 22952449
anti-VSG3	Lab internal	Pinger et al.[15]; PMID: 22952449
VSG2 antisera	This paper	N/A
VSG3 antisera	This paper	N/A
Recombinant monoclonal antibodies from the antibody repertoires	This paper	N/A
Rat anti-mouse CD19-BV421	Biolegend	Cat#115549; RRID: AB_2563066
Rat anti-mouse CD138-BV510	Biolegend	Cat#142521; RRID: AB_2562727
Rat anti-mouse IgG1-BV650	Biolegend	Cat#406629; RRID: AB_2716013
Goat anti-mouse IgM-Biotin	Jackson Laboratories	Cat#115-065-020; RRID: AB_2338560
Streptavidin-BV785	Biolegend	Cat#405249; PMID: 27841852
7-Aminoactinomycin D (7AAD)	Invitrogen	Cat#A1310; PMID: 1194669
Rat anti-mouse IgM-FITC	Biolegend	Cat#406506; RRID: AB_315056
Mouse anti-human IgG1-AlexFluor488	Invitrogen	Cat#A-10631; RRID: AB_2534050
Purified rat anti-mouse CD16/CD32 (Mouse BD Fc Block)	BD Pharmingen	Cat#553141; RRID: AB_394656
Bacterial and virus strains		
Subcloning Efficiency™ DH5α competent cells (E. coli)	Invitrogen	Cat#18265017
Chemicals, peptides, and recombinant proteins		
Dulbecco's Modified Eagle Medium (DMEM)	Sigma-Aldrich	Cat#D6429
FreeStyle 293 Expression Medium	Gibco	Cat#12338018
HMI-9 medium	PAN Biotech	Cat#so-15701
Nutridoma-SP	Roche	Cat#11011375001
OptiMEM	Gibco	Cat#31985062
RPMI-1640 medium	Sigma-Aldrich	Cat#R8758
Dulbeccos Phosphate Buffered Saline (DPBS)	Sigma-Aldrich	Cat#D8537
Fetal Bovine Serum (FBS)	Gibco	Cat#10270-106
Penicillin-Streptomycin	Sigma-Aldrich	Cat#P4333
Lipofectamine 2000	Invitrogen	Cat#11668027
293fectin	Thermo Fisher	Cat#12347-019
L-cysteine	Serva	Cat#17769
β-mercaptoethanol	Sigma-Aldrich	Cat#60-24-2
LB-broth (Miller)	Sigma-Aldrich	Cat#L3522
BglII restriction enzyme	New Engand Biolabs (NEB)	Cat#R0144S
EcoRV restriction enzyme	New Engand Biolabs (NEB)	Cat#R0195S
Endoproteinase LysC	New England Biolabs (NEB)	Cat#P8109S
PNGaseF	New England Biolabs (NEB)	Cat#P0704S
Trypsin-ultra™, Mass Spectrometry Grade	New England Biolabs (NEB)	Cat#P8101S
Blasticidin	Fisher Bioreagents	Cat#BP2647-100
Hygromycin	Thermo Fischer	Cat#10687010
Agarose	Roth	Cat#3810.4
Ammonium acetate	AppliChem	Cat#A2936
Calcium chloride ($CaCl_2$)	Roth	Cat#A119.1
Chelex 100 Resin	Biorad	Cat#1421253

(*Continued on next page*)

Continued

REAGENT or RESOURCE	SOURCE	IDENTIFIER
Diminazene aceturate (Berenil)	Abcam	Cat#908-54-3
Disodium hydrogen phosphate (Na_2HPO_4)	Applichem	Cat#A4732.1000
Ethylenediamine tetraacetic acid disodiumsalt.2H2O (EDTA)	Roth	Cat#X986.1
HEPES	Roth	Cat#9105.4
Imidazole	Roth	Cat#X998.4
Glucose	Acros	Cat#410950010
Glycerol	Sigma-Aldrich	Cat#G2025
Magnesium sulfate heptahydrate ($MgSO_4$)	Roth	Cat#8283.2
PEG400	Merck	Cat#8.07485
PEG3350	Sigma-Aldrich	Cat#202444
PEG8000	Jena Bioscience	Cat#CSS-256
Polyoxyethylenesorbitan monolaurate (Tween20)	Sigma-Aldrich	Cat#P9416
Potassium acetate	Roth	Cat#T874.5
Potassium chloride (KCl)	Roth	Cat#6781.1
Sodium chloride (NaCl)	Roth	Cat#3957.1
Sodium dihydrogen phosphate (NaH_2PO_4)	Applichem	Cat#A1373.1000
Sodium Dodecylsulfate (SDS)	Panreac Applichem	Cat#A2263
Trifluoroacetic acid (TFA)	Biosolve	Cat#202341
Trizma base	Sigma-Aldrich	Cat#93350
Zinc chloride ($ZnCl_2$)	Merck	Cat#7646-85-7
Ni-NTA	Qiagen	Cat#30210
Q-sepharose fast flow	GE Healthcare	Cat#17-0510-01
Critical commercial assays		
FITC Conjugation Kit - Lightning-Link	Abcam	Cat#ab188285
NEBuilder HiFi DNA Assembly kit	New England Biolabs	Cat#E5520S
NucleoSpin Gel and PCR clean-up kit	Macherey-Nagel	Cat#740609.50
Phusion High-Fidelity DNA Polymerase	New England Biolabs	Cat#M0530S
ProtoScript II First Strand cDNA Synthesis	New England Biolabs	Cat#E6560S
Q5 High-Fidelity DNA Polymerase kit	New England Biolabs	Cat#E0555S
Q5 Site-Directed Mutagenesis Kit	New England Biolabs	Cat#E0554S
RNeasy Mini kit	Qiagen	Cat#74104
TURBO DNA-free kit	Invitrogen	Cat#AM1907
All repertoire/antibody cloning reagents were the same as prevously published	Prof. Dr. Hedda Wardemann	Tiller et al.[18]; PMID: 17996249
Deposited data		
$VSG2_{WT}$ crystal structure	This paper	PDB ID: 7P56
$VSG2_{AAA}$ crystal structure	This paper	PDB ID: 7P57
$VSG3_{WT}$ crystal structure	This paper	PDB ID: 7P59
$VSG3_{S317A}$ crystal structure	This paper	PDB ID: 7P5A
$VSG3_{S319A}$ crystal structure	This paper	PDB ID: 7P5B
$VSG3_{SSAA}$ crystal structure	This paper	PDB ID: 7P5D
VSG3 MS data	This paper	ID: PXD027384
Experimental models: Cell lines		
Trypanosoma brucei brucei 224KI	Lab internal	Pinger et al.[27]; PMID: 29988048
Trypanosoma brucei brucei 224S317A	Lab internal	Pinger et al.[27]; PMID: 29988048
Trypanosoma brucei brucei 2T1	Prof. Dr. David Horn	Alsford et al.[39]; PMID: 16182389
HEK293T	ATCC	Cat#CRL-3216
FreeStyle HEK293F	Thermo Fisher	Cat#R79007

(*Continued on next page*)

Continued

REAGENT or RESOURCE	SOURCE	IDENTIFIER
Experimental models: Organisms/strains		
Trypanosome:*Trypanosoma brucei brucei*: Lister 427	Prof. Dr. David Horn Lab internal	Alsford et al.[39]; PMID: 16182389 Pinger et al.[27]; PMID: 29988048
Mouse: C57BL/6JRj$^{a/a}$: wild type	Janvier	Cat#C57BL/6JRj
Bacteria: *E. coli:* DH5a	Invitrogen	Cat#18265017
Oligonucleotides		
FAB_pFAB1_Fw: CTACGCGACACGTACGCG	This paper	N/A
FAB_pFAB1_Rv:CAGAACACAAAATCTCGGCTG	This paper	N/A
FAB_pFAB4_Fw: GCAGATGCAGCCAACAATTTCCAC GCAGCAGCAGCCGAATGCAGGCTAGCCAGTGGGC	This paper	N/A
FAB_pFAB4_Rv: GCCCACTGGCTAGCCTGCATTCG GCTGCTGCTGCGTGGAAATTGTTGGCTGCATCTGC	This paper	N/A
mut_S319A_Fw: AGGCAGCGCAgccGAAGGCTTATGTG	This paper	N/A
mut_S319A_Rv: GTGCAGCCTGTCGCTTTG	This paper	N/A
mut_SSAA_Fw: agccGAAGGCTTATGTGTCGAATACACTGC	This paper	N/A
mut_SSAA_Rv: gcggcGCCTGTGCAGCCTGTCGC	This paper	N/A
pAG_screen_Fw: CCCACAATATTTTAATTACTCTT GAAGATTGTAG	This paper	N/A
pAG_screen_Rv: GTTGATTGTAGCCGTTGCTCTT	This paper	N/A
panVSG-Fw (SL primer): ACAGTTTCTGTACTATATT	This paper	N/A
panVSG-Rev (3UTR primer): GATTTAGGTGACACT ATAGTGTTAAAATATATC	This paper	N/A
dNTP mix (10mM each) – 1mL	Thermo Fisher	Cat#R0192
All primers used for the repertoires have been listed before	Prof. Dr. Hedda Wardemann	Tiller et al.[18]; PMID: 17996249
Recombinant DNA		
pFAB1 ($VSG2_{WT}$)	This paper	N/A
pFAB4 ($VSG2_{AAA}$)	This paper	N/A
p224KI ($VSG3_{WT}$)	Lab internal	Pinger et al.[27]; PMID: 29988048
p224S317A ($VSG3_{S317A}$)	Lab internal	Pinger et al.[27]; PMID: 29988048
pAG1 ($VSG3_{S319A}$)	This paper	N/A
pAG2 ($VSG3_{SSAA}$)	This paper	N/A
All plasmids used for the repertoires have been listed before	Prof. Dr. Hedda Wardemann	Tiller et al.[18]; PMID: 17996249
Software and algorithms		
FlowJo (v10)	Tree Star	RRID:SCR_008520
GraphPad Prism (v9.3.1)	GraphPad Software	RRID:SCR_002798
Phenix (v. 1.19.2-4158)	Adams et al.[40]	http://www.phenix-online.org/; RRID:SCR_014224
Phaser (v. 2.8.3)	Phenix	https://www.phenix-online.org/documentation/reference/phaser.html; RRID:SCR_014219
CCP4 Software Suit	Collaborative Computational Project, Number 4, 1994	http://legacy.ccp4.ac.uk; RRID:SCR_007255
RAPD	NECAT	https://necat.chem.cornell.edu/RAPDMain
PEAQ ITC Analysis	Malvern Panalytical	http://www.malvernpanalytical.com/de/
Coot (v 0.9.6)	Emsley et al.[41]	RRID:SCR_014222
ChimeraX (v. 1.2.5)	Pettersen et al.[42]	RRID:SCR_015872
Other		
HiLoad 16/600 Superdex 200pg	GE Healthcare/Cytiva	Cat#28989335
AKTA Pure System	GE Healthcare	Cat#29018224
Amicon Stirred Cell	Merck	Cat#UFSCO5001

(*Continued on next page*)

Continued

REAGENT or RESOURCE	SOURCE	IDENTIFIER
Amicon Filtration Membrane	Merck	Cat#UFC901024
Crystalgen SuperClear Plates pregreased	Jena Bioscience	Cat#CPL-132
FrameStar PCR plates, 384-well, skirted	4titude	Cat#4TI-0384

RESOURCE AVAILABILITY

Lead contact

Further information and requests for resources and reagents should be directed to and will be fulfilled by the lead contact, Nina Papavasiliou (n.papavasiliou@dkfz-heidelberg.de).

Materials availability

Plasmids, constructs, and antibodies from this study can be obtained upon request.

Data and code availability

- Crystal structures that support the findings of this study have been deposited in RCSB Protein Data Bank with IDs: 7P56 ($VSG2_{WT}$), 7P57 ($VSG2_{AAA}$), 7P59 ($VSG3_{WT}$), 7P5A ($VSG3_{S317A}$), 7P5B ($VSG3_{S319A}$), 7P5D ($VSG3_{SSAA}$); Mass spectrometry data are available via ProteomeXchange with identifier PXD027384; Full repertoire sequences are available from the corresponding authors upon reasonable request.
- This paper does not report original code.
- Any additional information required to reanalyze the data reported in this paper is available from the lead contact upon request.

EXPERIMENTAL MODEL AND SUBJECT DETAILS

Trypanosome cell lines

All trypanosome cell lines used in this study were bloodstream-form trypanosomes derived from the Lister-427 "2T1" cell line[39] and were cultivated *in vitro* in HMI-9 medium[43] (formulated as described by PAN Biotech without FBS, l-cysteine or β-mercaptoethanol), supplemented with 10% fetal calf serum (Gibco), l-cysteine and β-mercaptoethanol. Cells were cultured at 37 °C and 5% CO_2. The $VSG3_{WT}$ and $VSG3_{S317A}$ cell lines were described before.[27] Isogenic $VSG3_{S319A}$ and $VSG3_{SSAA}$ mutant clones were derived from transfection of 2T1 (VSG2 expressing) cells with the pAG plasmids described in the methods, and then initially selected based on loss of VSG2 expression and gain of VSG3 expression (by FACS, see STAR Methods). Derivation of isogenic $VSG2_{WT}$ or $VSG2_{AAA}$ mutant trypanosomes was achieved through transfection of naturally occurring switchers of 2T1 (expressing VSG3, or VSG9) with the relevant pFAB plasmids (see STAR Methods), and then initially selected based on gain of VSG2 expression.

HEK 293T and 293F cell lines

HEK293T cells were obtained from ATCC (Cat#: CRL-3216) and maintained at 37 °C and 5-8% CO_2 in Dulbecco's Modified Eagle Medium (DMEM) (Sigma-Aldrich, Cat#: D6429) supplemented with 10% FBS and 1% Penicillin-Streptomycin (Sigma-Aldrich, Cat#: P4333). Cells were kept at 1-1.2x10^6 cells/mL prior to transfection and expanded accordingly for transfection purposes.

FreeStyle HEK293F cells were obtained from Thermo Fisher (Cat#: R79007) and maintained in FreeStyle 293 Expression Medium (Gibco, Cat#: 12338018). Cells were incubated at 37 °C and 5-8% CO_2 on a shaking platform operating at 120–130 rpm. Cells were kept below 1x10^6 cells/mL and expanded accordingly for transfection purposes.

Mouse strains

The aforementioned trypanosome cell lines were used to infect female, wild-type C57BL/6J mice, aged 6–8 weeks at experiment start (Janvier). Mice were kept in IVC cages under SPF conditions in the animal facility at the German Cancer Research Center (DKFZ, Heidelberg). All animal experiments were performed in accordance with institutional and governmental regulations under the German Animal Protection Law (§8 Tierschutzgesetz), and were approved by the Regierungspräsidium, Karlsruhe, Germany, under the protocol number G81-18.

Bacteria

E.coli strain DH5a was grown in LB-broth (Miller) medium (Sigma-Aldich, Cat#: L3522)for cultivation and plasmid purification. Cells were incubated at 37°C in plate or shaking incubators (180 rpm).

CellPress
OPEN ACCESS

METHOD DETAILS

Plasmids used to generate isogenic *T. brucei* clones

Plasmids used to generate $VSG3_{WT}$ and $VSG3_{S317A}$ -expressing cells were described in.[27] Modifications of these plasmids using site-directed mutagenesis (Q5, New England Biolabs) were used to generate $VSG3_{S319A}$ (pAG1) and the $VSG3_{SSAA}$ -expressing cells (pAG2). Plasmids were first linearized by EcoRV (New England Biolabs), and then transfected into VSG2-expressing cells (2T1).

Plasmids used to generate VSG2 and $VSG2_{AAA}$ isogenic strains (pFAB1 and pFAB4 respectively) were created using vector pSY371D-CTR-BSD[15] as a backbone (also modified to contain the hygromycin-resistance gene (HYG) instead of blasticidin). pFAB1 and pFAB4 were linearized with BglII (New England Biolabs) prior to transfection.

T. brucei transfections and verification

All transfections were performed using 10ug of each plasmid mixed with 100ul of 2.5-3x10^7 cells in homemade Tb-BSF buffer (90mM Na_2HPO_4, pH 7.3, 5mM KCl, 0.15mM $CaCl_2$, 50mM HEPES, pH7.3), using the AMAXA nucleofector (Lonza) program X-001, as previously described.[44] After 6h, blasticidin at a concentration of 100ug/ml ($VSG3_{S319A}$ and $VSG3_{SSAA}$ cell lines) or hygromycin at 25ug/ml ($VSG2_{WT}$ and $VSG2_{AAA}$ cell lines) were added and single-cell clones were obtained by serial dilutions in 24-well plates and harvested after 5 days. The $VSG3_{S319A}$ and $VSG3_{SSAA}$ clones were screened by FACS for VSG3 expression and VSG2 loss of expression and $VSG2_{WT}$ and $VSG2_{AAA}$ clones for VSG2 expression using monoclonal antibodies against these VSGs.[15] Positive clones were sequenced by isolating RNA using the RNeasy Mini Kit (Qiagen), followed by DNAse treatment with the TURBO DNA-free kit (Invitrogen) and cDNA synthesis with ProtoScript II First Strand cDNA Synthesis (New England Biolabs). The sequences were then amplified, using Phusion High-Fidelity DNA Polymerase (New England Biolabs), a forward primer binding to the spliced leader sequence and a reverse binding to the VSG 3′untranslated region. The final products were purified by gel extraction from a 1% gel with the NucleoSpin Gel and PCR clean-up kit (Macherey-Nagel) and sent for Sanger sequencing.

Spleen and antisera collection

6-8-week-old C57BL/6J wild-type mice were injected intraperitoneal (i.p.) with 1 × 10^3 parasites in HMI-9. Mice that cleared $VSG3_{S317A}$ infections naturally, were injected i.p. with 100 parasites in HMI-9. Mice treated with diminazene underwent an injection (i.p.) of 250 ng diminazene aceturate (Abcam)/mouse 4 days after infection, and this procedure was repeated after 24 h. On day 8 post parasite injection, mice were euthanized with CO2. Mice that naturally cleared the first peak of parasitemia were carefully monitored three times per day between days 5-7 post infection and euthanized with CO2 upon clearance of parasitemia.

After mice were euthanized, blood was collected via cardiac puncture and serum was separated from whole blood using Microtainer SST serum collection tubes (BD 365968). Spleen was also collected and single-cell suspensions were prepared by standard procedures.

Flow cytometry and single cell sorting

Splenocytes from spleens of Trypanosome-infected mice were thawed, washed in RPMI media (Gibco) at room temperature, centrifuged at 2000 rpm for 5 min and resuspended in 100ul 2% FBS/PBS. Cells were stained with rat anti-mouse CD19-BV421 (1:100, Biolegend), rat anti-mouse CD138-BV510 (1:300, Biolegend), rat anti-mouse IgG1-BV650 (1:100, Biolegend) and goat anti-mouse IgM-Biotin (1:400, Jackson Laboratories) for 45 min on ice in the dark. Biotin was detected using Streptavidin-BV785 (1:400, Biolegend) and 7-Aminoactinomycin D (7AAD) (1:200, Invitrogen) was used as a dead cell marker in all samples. The cells were analyzed on a LSRFortessa instrument (BD Bioscience), single-cell sorted into 384-well plates (black frame, 4titude) using either an Aria I or Aria Fusion II cell sorter (BD Bioscience) and analyzed using FlowJo software (v10). For single-cell sorting, the plasma cell population was defined as $7AAD^-CD19^{lo}CD138^+$ and was checked for IgM and IgG1 surface expression, without including these markers in the gating of the sort population. The exact isotype of each plasma cell was determined later by sequence analysis.

To assess binding of antisera to live trypanosomes, 1 x 10^6 parasites were harvested and incubated with $VSG2_{WT}$ anti-sera (1:4000) or $VSG2_{AAA}$ (1:2000) together with Fc block (1:200, BD Pharmingen) in cold Trypanosome Dilution Buffer (TDB) (5mM KCl, 80mM NaCl, 1mM $MgSO_4$, 20mM Na_2HPO_4, 2mM NaH_2PO_4, 20mM glucose, pH 7.4) for 10 min at 4°C. Cells were washed once with cold TDB and resuspended in 200μl cold TDB with rat anti-mouse IgM-FITC (1:500, Biolegend). Upon a single wash with cold TDB, cells were resuspended in 250μl TDB and immediately analyzed with FACSCalibur (BD Bioscences) and plotted using FlowJo software (v10).

To verify whether the repertoire antibodies that were produced in HEK cells were able to bind to live trypanosomes, 0.5 x 10^6 parasites were harvested, washed once with cold HMI-9 without FBS and stained in 200ul of each antibody supernatant for 10 min at 4°C. Cells were pelleted, resuspended in 100ul cold HMI-9 without FBS with mouse anti-human IgG1-AlexFluor488 (1:500, Invitrogen) for 10 min at 4°C in the dark. Cells were washed once with cold HMI-9 without FBS, resuspended in 100ul of the same buffer and immediately analyzed with FACSCalibur (BD Bioscences) and FlowJo software (v10).

Antibody repertoires and production of antibodies

Ig heavy (IgH), kappa (Igκ) and lambda (Igλ) genes from single plasma cells were amplified as described before.[18] Briefly, cDNA of each cell was produced using random hexameric primers and then the IgH, Igκ and Igλ gene transcripts were amplified by a

subsequent semi-nested PCR approach using V segment and constant region-specific primers.[18] The PCR products were sent for Sanger sequencing and analyzed with the IgBlast online tool (NCBI[45]) to generate the antibody repertoires. Matching heavy and light pairs originating from the same cell were picked, amplified using V and J gene-specific primers that include restriction sites for cloning and cloned into appropriate human expressing vectors.[18] After they were successfully cloned and their sequence was validated, the corresponding heavy and light chain plasmids were co-transfected into adherent HEK293T cells (ATCC) using Lipofectamine 2000 (Invitrogen) reagent in 1x OptiMEM (Gibco). After 6h the media was removed and cells were supplemented with 1x Nutridoma-SP (Roche). Supernatants containing the produced antibodies (as IgG1) were collected after 48h and 96h and tested for their ability to bind to live trypanosomes by FACS.

Fab cloning, expression and purification

Variable domains of Fab025, Fab207 and Fab239 heavy and light chains were cloned out of the human IgG1 vector templates mentioned above. Mouse expression vectors were generated via DNA Assembly (NEBuilder) using heavy and light chain vectors kindly provided by Mirjana Lilic. Heavy chains have a C-terminal hexa-histidine tag.

Fabs were then produced in HEK 293F cells by co-transfections of these cells with equal amounts of purified heavy and light chain plasmid, using 293fectin (Thermo Fisher 12347-019). Cells were incubated at 37 °C, 8% CO_2 on an orbital shaker at 130 rpm for 5 to 6 days. Supernatants were harvested by centrifugation at 1500xg for 15 minutes, filtered, concentrated in an Amicon stirred cell and diluted (2x) in binding buffer (50 mM Sodium Phosphate, 20 mM Imidazole, 300 mM NaCl, pH8). Supernatants were then incubated overnight with Ni-NTA agarose (Qiagen) at 4 °C. Next, gravity flow columns were used to collect the Ni-NTA agarose and columns were washed with binding buffer. Fabs were eluted with elution buffer (50 mM Sodium Phosphate, 300 mM NaCl, 250 mM Imidazole, pH8), concentrated in centrifugal units and re-suspended in Dulbecco's PBS. Samples were analyzed by SDS-PAGE.

Shannon entropy index calculation

Shannon entropy index on a sequence level or clonal diversity index, is a value that measures the frequency and quantity of plasma cell clones present in each sample. A value of 0.0 indicates clonal expansion, while a value of 1.0 complete diversity. Firstly, the sequences were categorized in clusters based on the presence of clones (e.g., if no clones were noted, the clusters were formed as 1, 2, 3, 4, etc., while in presence of clones as 1, 1, 1, 4, 4, 5, 5, etc.) and then the diversity index was calculated in R Studio (v2022.07.1 + 554) with "v" as the input file and the script:

```
> shannon.entropy <- function(p)
> {freq <- table(p)/sum(!is.na(p))
vec <- data.frame(freq)[,2]
-sum(log2(vec)*vec)}
> total <- sum(!is.na(v))
shannon.entropy(v)/log2(total)
```

VSG purification

VSGs were purified as described in[25] with minor changes. Briefly, cells grown to a density of 2.5-4 × 10^6 were centrifuged and lysed in 0.2mM $ZnCl_2$. Following cell lysis, the mixture was centrifuged and the pellet containing the VSG protein was resuspended in pre-warmed (40°C) 20mM HEPES buffer, pH 8.0, supplemented with 150mM sodium chloride ($VSG2_{WT}$ and $VSG2_{AAA}$) or 20mM HEPES buffer, pH 7.5, supplemented with 150mM sodium chloride ($VSG3_{WT}$ and the three sugar-mutants). After a second centrifugation, the supernatants containing the VSG protein were loaded onto an anion-exchange column (Q Sepharose Fast Flow, GE Healthcare) previously equilibrated with the respective HEPES buffer as above. The flow-through and two washes containing the VSG of interest were collected and concentrated using an Amicon Stirred Cell (Merck Millipore) and the sample was then run over a gel filtration column (Superdex 200, GE Healthcare) after equilibration with the respective HEPES buffer as above. Aliquots of both the different purification steps and the gel filtration runs were subjected to SDS-PAGE analysis for visual inspection (Figures S4C–S4H). From the gel filtration step onwards, all VSG3 constructs were gradually carboxy-terminal (CTD) truncated, likely due to cleavage by endogenous proteases, resulting in the crystallization of only the N-terminal domain. For crystallization of $VSG2_{AAA}$, VSG purified from gel filtration was concentrated to 2.2mg/ml and left for 1 week at 4°C where the CTD was also truncated (again, likely due to endogenous proteases). $VSG2_{AAA}$ underwent a second gel filtration (Superdex 200, GE Healthcare) and was concentrated to 4.8mg/ml. For crystallization of $VSG2_{WT}$, VSG was first purified with the same protocol but using 20mM Tris, pH 8.0. After passage over an anion-exchange column, VSG was concentrated to 10mg/ml and passed over a gel filtration column (Superdex 200, GE Healthcare) equilibrated in 20 mM Tris pH 8.0. Aliquots from the gel filtration runs were subjected to SDS–PAGE analysis for visual inspection, and concentrated to 2.5mg/ml.

Crystallization and structural determination

Native crystals of $VSG2_{WT}$ were grown by vapor diffusion using hanging drops formed from mixing a 1:1 volume ratio of the protein with an equilibration buffer consisting of 0.1M K-acetate, 22% PEG8000. For cryoprotection, crystals were transferred directly into a buffer with a 25% PEG 8000, 0.1M K-acetate, 20% glycerol and flash-cooled immediately afterward to 100 K (−173.15 °C). Data were collected at Advanced Photon Source (APS) at Argonne National Laboratory at beamline 24-ID-C and processed onsite through

the RAPD software pipeline. The structure was solved by molecular replacement using the model of PDB entry 1VSG with the PHENIX software suite.[40] The model was improved and finalized through several cycles of auto-building (PHENIX), manual adjustment, and refinement (PHENIX) (Table S1).

Native crystals of $VSG2_{AAA}$ were grown by vapor diffusion using hanging drops formed from mixing a 1:1 volume ratio of the protein with an equilibration buffer consisting of 0.1M Tris pH 8.0, 39% PEG400. This equilibration buffer is cryoprotective and crystals were flash-cooled afterward to 100 K (−173.15 °C). Data were collected at the Swiss Light Source (SLS) at a wavelength of 1.0Å on beamline X06DA (PXIII) The structure was solved by molecular replacement using the model of PDB entry 1VSG with the PHENIX suite.[40] The model was improved and finalized through several cycles of auto-building (PHENIX), manual adjustment, and refinement (PHENIX) (Table S1).

Purified $VSG3_{WT}$ and the three sugar-mutants were concentrated to 2 mg/ml in 20mM HEPES buffer, pH 7.5, supplemented with 150mM NaCl. Crystals were grown at 22°C by vapor diffusion using hanging drops with a 1:1 volume ratio of protein to equilibration buffer consisting of 21% PEG 3350, 250mM NaCl and 100mM Tris, pH 8.2 for $VSG3_{WT}$ and $VSG3_{S317A}$ and 25% PEG 3350, 300mM NaCl and 100mM HEPES, pH 7.5 for $VSG3_{S319A}$ and $VSG3_{SSAA}$. For cryoprotection the crystals were transferred to the same buffer as that used for equilibration but supplemented with 25% v/v glycerol and were flash-frozen in liquid nitrogen. Data for $VSG3_{WT}$, $VSG3_{S317A}$ and $VSG3_{SSAA}$ were collected at the Swiss Light Source (SLS) at a wavelength of 1.0Å on beamline X06DA (PXIII) and for $VSG3_{S319A}$ at the Diamond Light Source at a wavelength of 0.9763Å on beamline i03. The $VSG3_{WT}$ and sugar-mutant structures were obtained using the previously solved $VSG3_{WT}$ structure (PDB ID: 6ELC)[27] as a model to perform Molecular Replacement in the PHENIX suite.[40] The models were improved and finalized through several cycles of auto-building (PHENIX), manual adjustment, and refinement (PHENIX) (Table S2).

Mass spectrometry

Purified $VSG2_{WT}$ and $VSG2_{AAA}$ samples were buffer-exchanged into native Mass Spectrometry (nMS) solution (150mM ammonium acetate, 0.01% Tween-20, pH7.5) using Zeba desalting microspin columns with a 40-kDa molecular weight cut-off (Thermo Scientific). An aliquot (2–3μL) of the buffer-exchanged sample was loaded into a gold-coated quartz capillary tip that was prepared in-house. The sample was then electrosprayed into an Exactive Plus EMR instrument (Thermo Fisher Scientific) using a modified static nanospray source.[46] The MS parameters used included: spray voltage, 1.1 – 1.3kV; capillary temperature, 200°C; S-lens RF level, 200; resolving power, 35,000 at *m/z* of 200; AGC target, 1 – 3 x 10^6; number of microscans, 5; maximum injection time, 200ms; in-source dissociation (ISD), 200V; injection flatapole, 8V; interflatapole, 7V; bent flatapole, 6V; high energy collision dissociation (HCD), 10V; ultrahigh vacuum pressure, 5×10^{-10} mbar; total number of scans, 100. Mass calibration in positive mode was performed using cesium iodide. Raw nMS spectra were visualized using Thermo Xcalibur Qual Browser (version 4.2.47). Deconvolution was performed using UniDec version 4.2.[47,48] The UniDec parameters used were m/z range: 3,500 – 5,500; mass range: 90,000 – 105,000Da; sample mass every 0.2Da; smooth charge state distribution, on; peak shape function, Gaussian; and Beta softmax function setting, 20.

Native MS analyses of the purified VSG2 samples revealed massive heterogeneity due to extensive glycosylation consistent with previous studies that determined N-glycosylation at two Asn sites and variable galactosylation at the C-terminal GPI anchor per VSG2 monomer.[49–51] To reduce sample complexity and enable unambiguous identification of bound metal ions, the VSG samples were N-deglycosylated using PNGaseF (NEB) with and without 10mM EDTA at 37°C for 3 - 4h. The deglycosylated samples were then buffer exchanged and analyzed by nMS as described above.

The expected masses for the VSG2 glycoforms were determined as follows. The signal peptide at the N-terminus (residues 1-27) and the GPI attachment signal peptide at the C-terminus (residues 460-476) were removed from the precursor $VSG2_{WT}$ sequence yielding a monomer mass 46,291.8Da for the processed protein. Common to all the monomers is the presence of four disulfide bridges (-8.06 Da) as well as attachment of glucosamine-α1-6-myo-inositol-1,2-cyclic phosphate (+385.26 Da), ethanolamine phosphate (+123.05 Da) and five hexoses (+810.70 Da) at the C-terminal GPI anchor. Moreover, PNGaseF cleavage of N-linked glycans at two Asn residues results in deamidation of Asn to Asp (+1.97 Da). Overall, the resulting monomer and dimer masses are 47,604.7 Da and 95,209.4 Da, respectively. Each additional galactose attachment from variable galactosylation at the GPI anchor adds 162.14 Da. Each Ca^{2+} ion bound adds 38.06 Da (average mass of Ca minus the mass of $2H^+$ from deprotonation of two aspartic acids that coordinate with the cation). The DND-to-AAA mutation results in a decrease of $VSG2_{WT}$ dimer mass by 262.10 Da (Table S3).

Purified $VSG3_{WT}$ was either concentrated to 3mg/mL in 20mM HEPES, pH 8.0, with 150mM NaCl and sent for Electron transfer dissociation (ETD) analysis or 50ug of protein in the same buffer were treated as described in[27] and then separated by SDS PAGE. The 17 kDa fragment was excised and processed as described.[52] In brief, trypsin digestion was done overnight at 37°C. The reaction was quenched by addition of 20μL of 0.1% trifluoroacetic acid (TFA; Biosolve, Valkenswaard, The Netherlands) and the supernatant was dried in a vacuum concentrator before LC-MS analysis. Nanoflow LC-MS^2 analysis was performed with an Ultimate 3000 liquid chromatography system coupled to an Orbitrap Elite mass spectrometer equipped with ETD (Thermo-Fischer, Bremen, Germany). Samples were dissolved in 0.1% TFA, injected to a self-packed analytical column (75um x 200mm; ReproSil Pur 120 C18-AQ; Dr Maisch GmbH) and eluted with a flow rate of 300 nl/min in an acetonitrile-gradient (3% - 40%). The mass spectrometer was operated in data-dependent acquisition mode, automatically switching between MS and MS^2 Collision

induced dissociation MS^2 spectra were generated for up to 10 precursors with normalized collision energy of 29%. Electron transfer dissociation (ETD) MS^2 spectra were generated for up to 5 precursors using the default settings of the instrument. Each analysis was done in triplicate.

Raw files were processed using Proteome discoverer 2.2 (Thermo Scientific) for peptide identification and quantification. MS^2 spectra were searched against the Uniprot Trypanosoma database (UniprotKB), a custom database entry with the VSG3 sequence and the contaminants database (MaxQuant database; MPI Martinsried) with the following parameters: Acetyl (Protein N-term), Oxidation (M) and Hex (S,T) as variable modifications and carbamidomethyl (C) as static modification. Trypsin/P was set as the proteolytic enzyme with up to 2 missed cleavages allowed. The maximum false discovery rate for proteins and peptides was 0.01 and a minimum peptide length of 7 amino acids was required.

Isothermal titration calorimetry

To evaluate binding of ions to $VSG2_{WT}$ or $VSG2_{AAA}$ and remove contaminating calcium, all glassware was first treated with phosphoric acid and water to prepare all buffers and solutions for treatment with Chelex 100 Resin 200-400 mesh (BioRad). Upon purification of VSG2, the CTD was removed by digestion with Endoproteinase LysC (New England Biolabs) at a 1:500 LysC/substrate ratio by mass together with 10mM EDTA for 5h at 37°C. The samples were then run over a gel filtration column (Superdex 200, GE Healthcare) after equilibration with the respective 20mM Tris pH 8.0 buffer. Afterward, proteins were concentrated to 30mM by concentration in 10-kDa disposable ultrafiltration centrifugal devices.

ITC experiments were performed using a PEAQ ITC (Malvern) at 20°C with a stirring rate of 750 rpm. Titration buffers contained 20mM Tris pH 8. In each experiment, the protein concentration in the cell was 30μM. $CaCl_2$, KCl and $MgCl_2$ were injected at 600μM with injection sizes of 12 × 3μL. The data were baseline-corrected, integrated and analysed with the PEAQ ITC Analysis software (Malvern), fitted using a single-site binding model.

QUANTIFICATION AND STATISTICAL ANALYSIS

Statistical analysis for Figure 3B and Table S4 were performed in GraphPad Prism (v9.3.1). For Figure 3B the Brown-Forsythe and Welch ANOVA tests followed by Dunnett's multiple-comparison test was used, while for Table S4 Fischer's exact test was performed. Differences were determined as significant when $p < 0.05$.